Stabilized D_2R G-protein coupled receptor oligomers identify multi-state β-arrestin complexes

Katie L. Sharrocks[1,3], Francesca Fanelli[2], Yewei Lui[1], Annabelle J. Milner[3], Wu Yining[1], Bernadette Byrne[1*], Aylin C. Hanyaloglu[3*]

[1]Department of Life Sciences, Imperial College London, UK

[2]Department Life Sciences, University of Modena and Reggio Emilia, Modena, Italy

[3]Department of Metabolism, Digestion and Reproduction, Imperial College London, UK

*To whom correspondence should be addressed: b.byrne@imperial.ac.uk, a.hanyaloglu@imperial.ac.uk

Keywords: GPCR; D2 dopamine receptor; arrestin; β-arrestin-2; dimer; oligomer; internalization; single-molecule imaging; molecular modelling; signaling

ABSTRACT

The G-protein coupled receptor (GPCR) superfamily directs central roles in many physiological and pathophysiological processes via diverse and complex mechanisms. GPCRs can exhibit signal pleiotropy via formation of di/oligomers both with themselves and other GPCRs. A deeper understanding of the molecular basis and functional role of oligomerization would facilitate rational design of activity-selective ligands. A structural model of the D2 dopamine receptor (D_2R) homomer identified distinct combinations of substitutions likely to stabilize protomer interactions. Molecular modelling of β-arrestin-2 (βarr2) bound to predicted dimer models suggests a 2:2 receptor:βarr2 stoichiometry, with the dimer favouring βarr2 over Gαi coupling. A combination of biochemical, biophysical and super-resolution, single molecule imaging approaches demonstrated that the D_2R mutant homomers exhibited greater stability. The mutant D_2R homomers also exhibited bias towards recruitment of the GPCR adaptor protein βarr2 with either faster or ligand-independent βarr2 recruitment, increased internalization and reprogrammed regulation of ERK signaling. Through GPCR dimer-stabilization, we propose that D_2R di/oligomerization has a role in βarr2-biased signaling.

34 **INTRODUCTION**

35 G-protein coupled receptors (GPCRs) are the largest family of proteins in mammals,
36 expressed in a range of cell types, and regulate a diverse set of physiological
37 processes[1]. They are the targets of approximately 35% of current FDA approved drugs
38 and remain major drug discovery targets[2,3]. GPCRs can regulate several intracellular
39 signaling cascades through coupling with distinct heterotrimeric G-proteins. In
40 addition, GPCRs can diversify their signaling through the multi-functional adaptor
41 proteins, the non-visual arrestins; β-arrestin-1 and 2 (βarr1 and βarr2, respectively,
42 also known as arrestins 2 and 3)[4,5].In addition to uncoupling GPCRs from their
43 heterotrimeric G-proteins, and driving receptor internalization via clathrin-coated pits,
44 βarr1/2 can mediate distinct cellular pathways through activation of signaling such as
45 the mitogen-activated protein kinase (MAPK) pathway [4,5].
46
47 Class A 'rhodopsin-like' GPCRs can function as monomers, however increasing
48 biophysical, computational, pharmacological and physiological evidence suggests that
49 they can form both homomers and heteromers with other GPCRs[6–12]. A dynamic
50 equilibrium between monomers and transient di/oligomers has been reported for
51 several GPCRs[13–16]. Oligomerization can impact the function of receptors, altering
52 ligand efficacy, G-protein activation or preference for G-protein coupling selectivity[17–
53 20]. The impact of oligomerization on GPCR/β-arr function is less clear but a recent
54 study demonstrated that oligomerization of platelet-activating factor receptor (PAFR)
55 decreases βarr recruitment and conversely, βarr seemed to decrease oligomerization
56 of the receptor[21]. β_2AR has also been shown to dimerise in a βarr-dependent manner
57 upon stimulation with a βarr-biased ligand[22]. This highlights the potential for
58 oligomerization to dramatically influence all aspects of GPCR signaling.

59

60 Structural biology remains an important area for uncovering GPCR activation and
61 dimerization mechanisms[23], yet there have been limited reports of high-resolution
62 structures of Class-A GPCR dimers/oligomers. Transmembrane domains often play a
63 key role in dimer interfaces, with the most recurrent interfaces involving helix 1 (H1).
64 Indeed, H1-H1 contacts were found in homo-dimeric rhodopsin (PDB: 2I36, 2I37,
65 3CAP, and 6OFJ), κ-opioid (PDB: 4DJH), β1-adrenergic (PDB: 4GPO), M3-muscarinic
66 (PDB: 5ZHP), EP3-prostanoid (PDB: 6AK3), AT1-angiotensin (PDB: 6DO1), and
67 apelin (PDBs 6WOL and 6WON) receptors. Furthermore, H1-H4 contacts were found
68 in homo-dimeric 5HT2A-serotonin (PDBs: 6WGT and 6WH4) and CCR5-chemokine
69 (PDBs: 4MBS and 6AKX) receptors, whereas H1-H5 contacts were found in homo-
70 dimeric D4 dopamine receptor (PDB: 6IQL). Homodimers characterized by H4-H5 or
71 H4-H6 H5-H5, or H6-H7 were found for CXCR4, β1-AR, C5a1, CCR2, α2C-AR and
72 CysLT1 receptors (PDBs: 3ODU/3OE8/3OE9, 5F8U, 5O9H, 6GPX, 6KUW, 6RZ5,
73 respectively).

74

75 The D_2 dopamine (D_2R) is a class A 'rhodopsin-like' GPCR, coupling to $G\alpha_{i/o}$[24]. The
76 primary physiological roles of D_2R in the brain are regulation of locomotion, and in
77 reward and reinforcement mechanisms[25], while pathophsyiologically this receptor is
78 implicated in a number of neurological diseases including schizophrenia and
79 Parkinson's Disease[26]. D_2R has been shown to form homodimers both in heterologous
80 expression systems at physiological expression levels and in native tissues[14,27–29].
81 Several antipsychotics target the D_2R/ βarr2 complex and an increase in D_2R
82 homodimers has been associated with schizophrenia[30,31]. Thus, D_2R complexes
83 represent excellent therapeutic targets. While there are several high-resolution

84 structures of monomeric D_2R, also in complex with G-protein[32–34], the lack of
85 information on precise molecular interactions between protomers and the absence of
86 high-resolution dimer structures has hindered the ability to specifically target these
87 complexes for therapeutic benefits.
88
89 Here we employed a convergent strategy to engineer distinct stabilized D_2R
90 homodimers. Residues were identified within the H1-H2 interface to enhance
91 homodimer/oligomer stability assessed biochemically, biophysically and via super-
92 resolution single molecule approaches. Interestingly, these engineered receptors also
93 exhibited a bias towards βarr2 associated pathways with either altered temporal
94 kinetics of ligand-mediated complexes, or functionally biased ligand-independent
95 GPCR-arrestin complexes. Docking of βarr2 to the predicted homodimers of wild type
96 (WT) or mutated D_2R provide insights into the signaling active supramolecular
97 assembly. This may highlight a novel selective role for D_2R homomers in promoting
98 distinct transitions to βarr2 association and signaling activity.
99

100 # RESULTS

101 ## D_2R mutations at the H2-H2 interface increase D_2R homodimer stability
102 and protomer proximity

103 To stabilize a D_2R homodimer, our experimental design was guided by molecular
104 modelling (see Methods). Simulations of D_2R homodimerization were carried out using
105 the structural models of either the inactive or the active states of the receptor. The
106 results shown here concern symmetrical D_2R homodimers with both protomers in their
107 active states (i.e. extracted from the 8IRS PDB structural complex between ritigotine-
108 bound D_2R and heterotrimeric Gαi)), since they were most reliable in terms of
109 membrane-topology indices . The predicted homodimer forms a symmetrical interface
110 characterized by contacts at the extracellular ends of H1-H1, H1-H2 and H2-H2 and
111 H1-H8, H8-H8 contacts on the cytosolic side (hereafter referred to as the H1, H2
112 dimer) (Fig. 1a). The stronger contacts from both protomers in the extracellular half of
113 the interface involve: a) Y36 (H1) and F102 (extracellular loop 1 (EL1)); b) T39 (H1)
114 and W90 (H2) and; c) T42 (H1) and I45 (H1) d) V97 (H2) from both protomers; and e)
115 V96 and Y93 (both in H2). The same interface was found for symmetric D_2R
116 homodimers with both protomers in the inactive state (i.e. extracted from the 6CM4
117 PDB structural complex of D_2R bound to risperidone) but not for asymmetric inactive-
118 active D_2R dimers. The presence of at least one protomer in the inactive state
119 produced an additional interface characterized, among others, by H4-H4 contacts. For
120 the H1,H2 dimer, we focused on the most extracellular amino acid residues to
121 potentially drive formation of disulphide bridges. To strengthen the contacts between
122 protomers at the interface, our models suggested mutations of Y93 to cysteine (Y93C),
123 V96 to either serine (V96S) or cysteine (V96C) and V97 to cysteine (V97C) alone or
124 in combination with V96S (V96S/V97C).

125 To assess the effect of these mutations on levels of di/oligomeric protein present in
126 cells, Western blot analysis under reducing or non-reducing conditions (in the
127 presence or absence of β-mercaptoethanol) was carried out. Under non-reducing
128 conditions receptors were primarily in a higher order, dimeric/oligomeric, complex
129 (>180 kDa) (Supplementary Fig. 1). Under reducing conditions, the majority of the WT
130 D_2R shifted in size predominately to a monomeric form (predicted size of FLAG-tagged
131 D_2R-Rluc8, ~90kDa with glycosylated D_2R-Rluc8 appearing at ~110kDa), however, a
132 greater proportion of V96C, V96S and in particular, V96S/V97C mutants, existed in a
133 higher order complex (Fig. 1b and c). Given the inability to distinguish between
134 different types of higher-order oligomeric complexes using SDS-PAGE, quantification
135 of only relative WT and mutant D_2R dimer proteins levels of were compared (Fig. 1b
136 and c). To directly measure receptor-receptor interactions in intact cells,
137 bioluminescence resonance energy transfer (BRET) saturation assays were carried
138 out. The WT D_2R exhibited a saturation profile indicating formation of homomers (Fig
139 1e-g and Supplementary Fig. 2a and 3a), as previously reported by BRET[28]. When
140 compared to WT D_2R, a significant increase in BRETmax in cells expressing D_2R
141 V96C, V96S or V96S/V97C (Figs. 1e-m), indicating an increase in protomer proximity
142 within D_2R homomers. No significant changes in the receptor interaction profile were
143 observed for Y93C (Supplementary Fig. 2b-d). All receptors exhibited a similar total
144 expression level (Supp Fig. 2e-h) This supports the data obtained by Western blot
145 analysis that the V96S/V97C mutation in particular may stabilize and/or increase the
146 proportion of D_2R homomers. There was no change in BRET50 (an indicator of
147 protomer-protomer affinity) relative to WT for any of the mutants. Treatment of cells
148 with the D_2R-selective agonist, quinpirole, did not significantly impact either the
149 BRETmax or BRET50 of WT or mutant D_2Rs (Supplementary Fig. 3). To further

150 understand how these sites impact receptor homomer interactions, computational
151 simulations of V96C (Mut1) and V96S/V97C (Mut2) homodimerization were carried
152 out and predicted that these mutated homodimers exhibit the same architecture as
153 WT, though in Mut2 the interface is tighter than in WT or Mut1 (Supplementary Fig. 4).
154 In the predicted Mut1 dimer, C96 interacts with both Y93 and C96 on the facing
155 protomer, whereas in the Mut2 dimer C97 interacts with C97 and S96 interacts with
156 Y93 on the facing protomer.
157

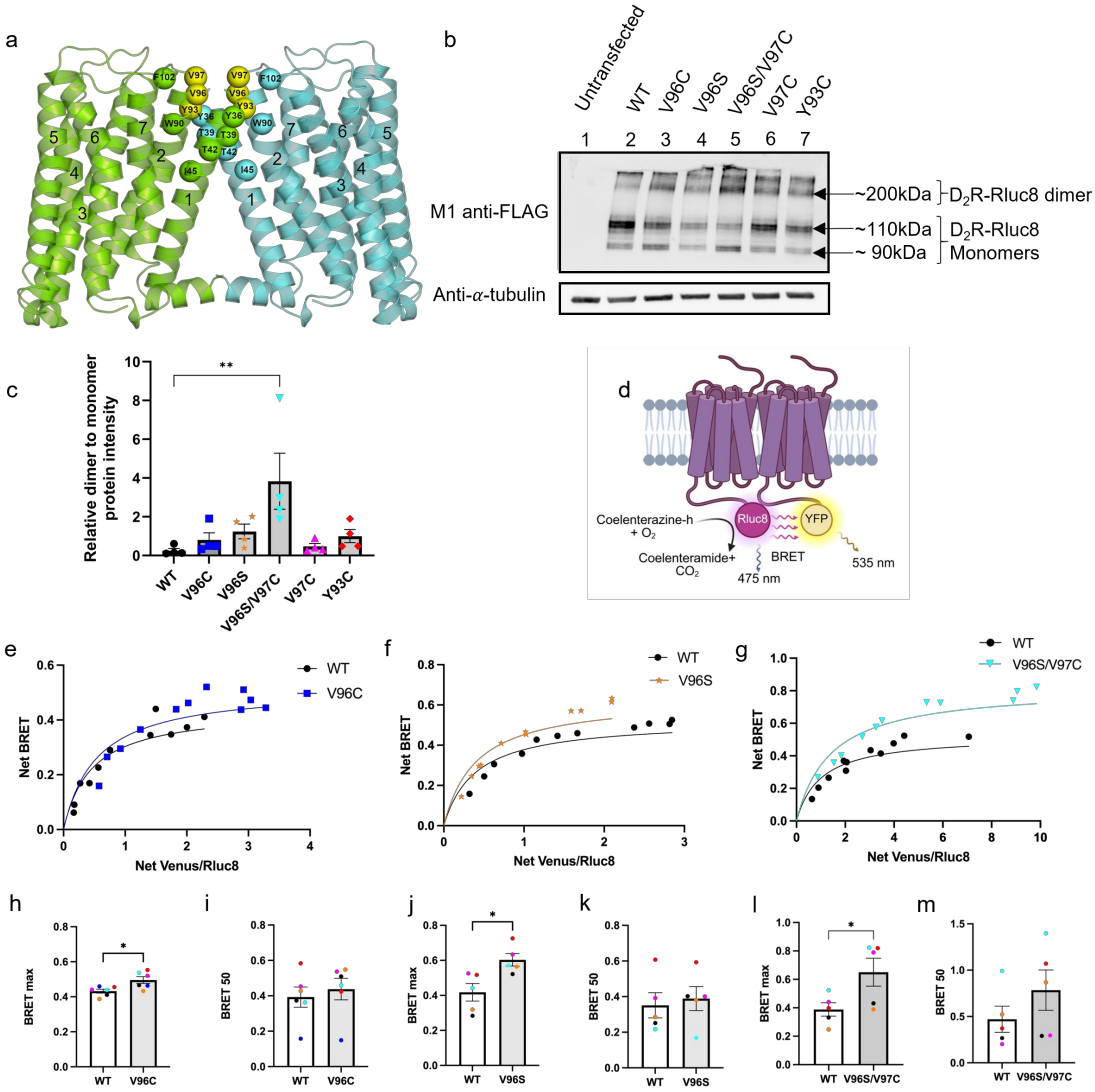

Fig.1. The impact of D_2R mutants identified from molecular docking simulations on homodimer stability. (a) The predicted WT D_2R homodimer (H1,H2 dimer) is shown in cartoon representation, with the two protomers coloured lemon-green and aquamarine. Interface amino acids are shown as spheres centred on the Cα-atoms. The mutated amino acids are highlighted in yellow. **(b)** Western blot analysis of HEK293 cell lysates transfected with WT or mutant D_2R-Rluc8 as stated, carried out under reducing conditions. Probed with M1 anti-FLAG to detect the FLAG tag at the N-terminus of receptor constructs (D_2R-Rluc8 monomer ~90kDa or ~110kDa with glycosylation) and anti-α-tubulin as a loading control. (**c**) Quantification of band intensity, represented as relative fold change of D_2R dimer levels (~200 kDa band) to monomer levels (~110 kDa) under reducing conditions, N=4, error bars are +/- SEM. Ordinary one-way ANOVA used to measure statistical differences, (p**=0.0051) (**d**) Schematic showing BRET assay. (**e**) Representative BRET saturation curve obtained from HEK293 cells expressing either D_2R WT (black), D_2R V96C (blue), (**f**) V96S (orange) or **(g)** V96S/V97C (cyan). Saturation curves were used to quantity BRETmax (**h, j, l**) and BRET50 values (**i, k, m**), colour coded for each individual experiment. N=5 for WT vs V96S and V96S/V97C or N=6 for WT vs V96C. Un-paired, two-tailed Student's t test used to measure statistical differences in BRET50 or BRETmax values between WT and mutant D_2R, (p*= 0.0186 (h) or 0.0162 (j) or 0.0432 (l)).

158

159 **Super-resolution imaging of cell surface D_2R at the single molecule**
160 **level reveals increased oligomerization in D_2R V96S/V97C mutants**

161 Both BRET and Western blot methods assess the total receptor population within a
162 cell, whether in the biosynthetic, plasma membrane, or endocytic compartments. To
163 quantitate the organisation of individual receptors at the plasma membrane,
164 photoactivated localization microscopy with photoactivatable dyes (PD-PALM) with
165 TIRF-imaging was employed. This single-molecule high-resolution technique gives
166 <10 nm resolution and has provided detailed information on plasma membrane
167 localised GPCRs in monomeric, dimeric or oligomeric forms[35–39]. PD-PALM imaging
168 was carried out on HEK 293 cells expressing WT or mutant D_2Rs and directly labelled
169 with an anti-FLAG antibody conjugated to CAGE 500 at a 1:1 ratio. Precise localisation
170 of individual receptors and subsequent processing through near neighbourhood
171 analysis enabled individual monomer or oligomer populations to be quantified (Fig. 2a
172 and b). Under basal conditions, the percentage of total receptors in a monomeric state
173 in D_2R V96S/V97C cells was significantly lower than WT D_2R (Fig. 2c). Additionally,
174 for V96S/V97C there was a corresponding significant increase in the proportion of
175 receptors in the di/oligomeric state compared to WT D_2R. When these di/oligomer
176 populations were assessed according to the number of receptors in the complex, this
177 revealed that these assemblies primarily involved receptor dimers (~17% of total
178 receptors), yet also a range of higher-order receptor oligomers. The increase in
179 associated V96S/V97C receptor was not attributed to enrichment of a specific
180 oligomer population but rather across receptor di/oligomers (Fig. 2d).
181
182 Following quinpirole stimulation, the different receptors exhibited distinct levels of
183 monomer and oligomeric complexes, compared to basal conditions (Fig. 2e-g).

184 Stimulation of D_2R WT expressing cells with quinpirole did not significantly alter the
185 proportion of receptors in an oligomeric complex. However, ligand activation of D_2R
186 V96S resulted in a significant decrease in the proportion of receptor in an oligomer
187 compared to both WT D_2R expressing cells whose complexes were not significantly
188 altered when stimulated with ligand (Fig. 2e and f). For V96S, this agonist-dependent
189 decrease in associated receptors was due to a decrease in receptor dimers (Fig. 2g).
190 While PD-PALM analysis suggests that quinpirole treatment may alter
191 di/oligomerization of certain D_2R mutants, quinpirole stimulation did not alter BRET
192 saturation profiles (Supplementary Fig. 3 and Supplementary Fig.5). This could reflect
193 that PD-PALM imaging quantifies complexes of cell surface receptors, while BRET
194 detects interactions across all subcellular compartments.
195
196 We have previously demonstrated that receptor density can influence oligomerization
197 for Class A GPCRs as measured by PD-PALM, particularly higher order complexes
198 (>5 receptors/oligomer[39]). For D_2R, the percentage of monomeric receptors was
199 inversely proportional to the receptor density (Supplementary Fig. 5a and b). While for
200 some GPCRs, receptor density impacts higher order complexes[39], our observation for
201 D_2Rs via super-resolution imaging is in line with other studies with D_2R_L using
202 diffraction-limited single molecule imaging, reporting a small but significant impact of
203 receptor density on the levels of monomer and di/oligomer distribution[14]. Therefore,
204 based on the correlation observed via PD-PALM analysis, the di/oligomeric state of
205 receptors were also analysed under 'high' (>100 receptors/μm^2) or 'low' (<100
206 receptors/μm^2) levels of expressed surface receptors, to understand the effect of
207 receptor density on homomer formations in WT and mutant receptors (Supplementary
208 Fig. 5b-h). In the absence of agonist, differences in complex formation between WT

209 and mutant receptors were independent of receptor density. The range of receptor
210 densities in cells treated with quinpirole was generally lower for cells expressing D_2R
211 V96S and V96C compared to WT or V96S/V97C, likely due to ligand-induced receptor
212 internalization (Supplementary Fig. 5b). This may partially account for the decrease in
213 oligomeric receptors in D_2R V96S or V96C compared to WT D_2R as when cells with
214 similar receptor densities were analysed, this decrease was not significant
215 (Supplementary Fig. 5g and h).
216
217 Taken together, this may suggest that the V96S/V97C mutant increases the propensity
218 for D_2R to form an oligomer. This is in line with docking simulations that predict a tighter
219 interface in the V96S/V97C dimer compared to the WT or the V96C dimer
220 (Supplementary Fig. 4). These results provide further evidence that the V96S/V97C
221 mutant D_2R may increase the stability of D_2R oligomers. While quinpirole stimulation
222 does not significantly alter the organization of D_2R complexes.
223

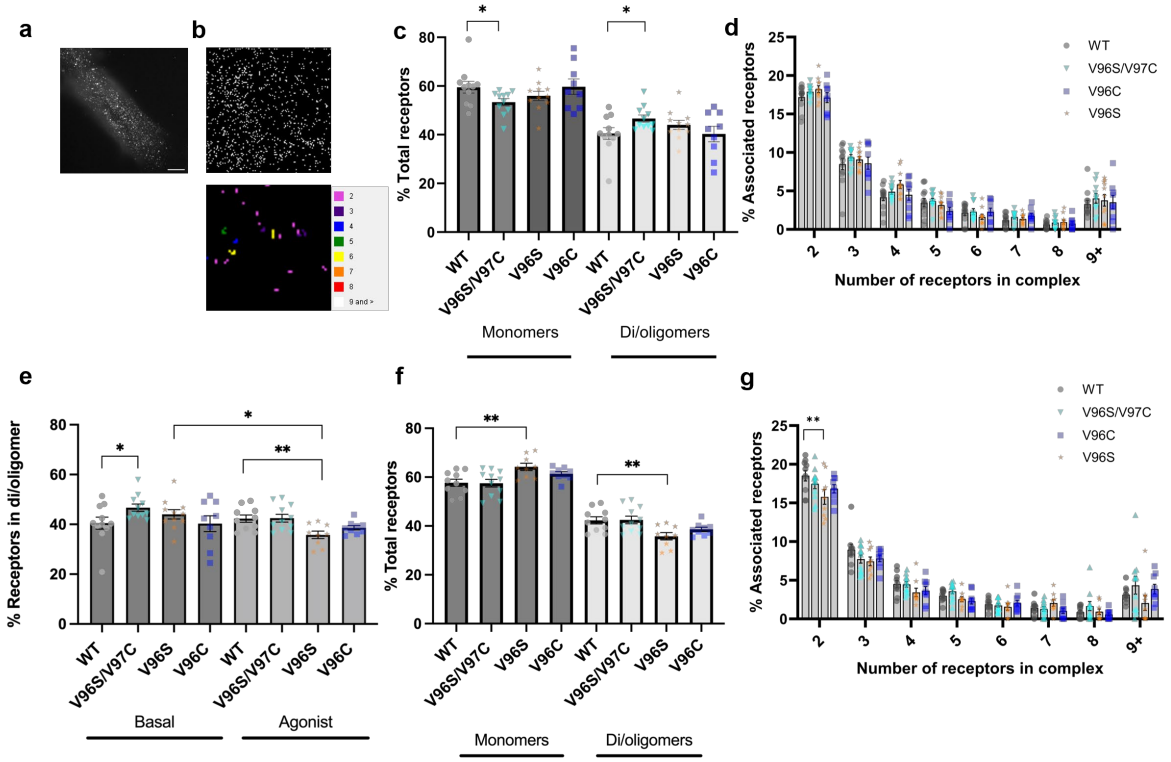

Fig. 2. PD-PALM super-resolution microscopy allows quantification of cell surface D_2R oligomers. (**a**) Representative image of HEK293 cells transiently transfected with FLAG-D_2R and labelled with FLAG-CAGE500, imaged over 20,000 frames by TIRF microscopy following uncaging and activation of the CAGE500 dye. Scale bar=50 µm. **b)** Representative PD-PALM 7 μm^2 image of FLAG-D_2R labelled with FLAG-CAGE500 with a heat map quantifying oligomer populations. (**c**) Proportion of D_2R WT or mutant receptors as monomers or in di/oligomeric complexes as a percentage of total receptors. (**d**) Composition of D_2R oligomers separated into number of receptors in the complex and expressed as a percentage of total receptors. (**e**) Proportion of associated receptors in di/oligomeric complexes, expressed as a percentage of total number of receptors under basal conditions or after 5 minutes 10 µM quinpirole stimulation. (**f**) Proportion of D_2R WT or mutant receptors as monomers or in di/oligomeric complexes as a percentage of total receptors after 5 minutes 10 µM quinpirole stimulation. (**g)** Composition of D_2R oligomers after 5 minutes 10 µM quinpirole stimulation prior to fixation, separated into number of receptors in the complex and expressed as a percentage of total receptors. Mean +/- SEM, N=3 individual experiments, 3-4 cells imaged for each independent repeat. In c, e and f unpaired, two-tailed Student's t test used to measure differences between WT and mutant D_2R ($p^*=0.042$ (c and e) or 0.0035 $p^{**}=0.0068$ (e and f)). In d and g two-way ANOVA followed by Šídák's multiple comparisons test used to measure statistical differences between WT and mutant D_2R in different receptor complexes ($p^{**}=0.0019$).

227 **D_2R mutants that stabilize homomeric interactions impact Gαi-**
228 **mediated signaling and βarr2 recruitment profiles**

229 Following the observation that some mutations increase the stability and/or degree of
230 D_2R homomers, the impact of these mutations on canonical Gαi signaling was
231 assessed. Forskolin-induced cAMP levels were measured in the presence of
232 quinpirole to assess inhibition of intracellular cAMP levels via D_2R-mediated Gαi
233 signaling. HEK293 cells expressing D_2R WT and stimulated with 1 μM quinpirole for
234 5, 15, or 30 minutes exhibited a decrease in forskolin-induced cAMP levels at all
235 agonist time points (Supplementary Fig. 6). This decrease in cAMP is specifically due
236 to D_2R-mediated signaling as untransfected HEK293 cells do not exhibit this decrease
237 upon quinpirole addition. Concentration-response curves in cells expressing WT or
238 mutant D_2R showed similar curves and EC_{50} values, suggesting that the potency of
239 quinpirole to activate D_2R/Gαi-mediated signaling pathways is not altered by these
240 mutations (Fig. 3a and Table 1). However, when the ligand-induced Gαi response was
241 calculated from the change in cAMP levels in cells treated with the minimum to the
242 maximum dose of quinpirole, the D_2R V96S/V97C mutant had significantly reduced
243 ligand-induced Gαi response compared to WT (Fig. 3b) suggesting a decrease in
244 efficacy for quinpirole in D_2R V96S/V97C expressing cells.

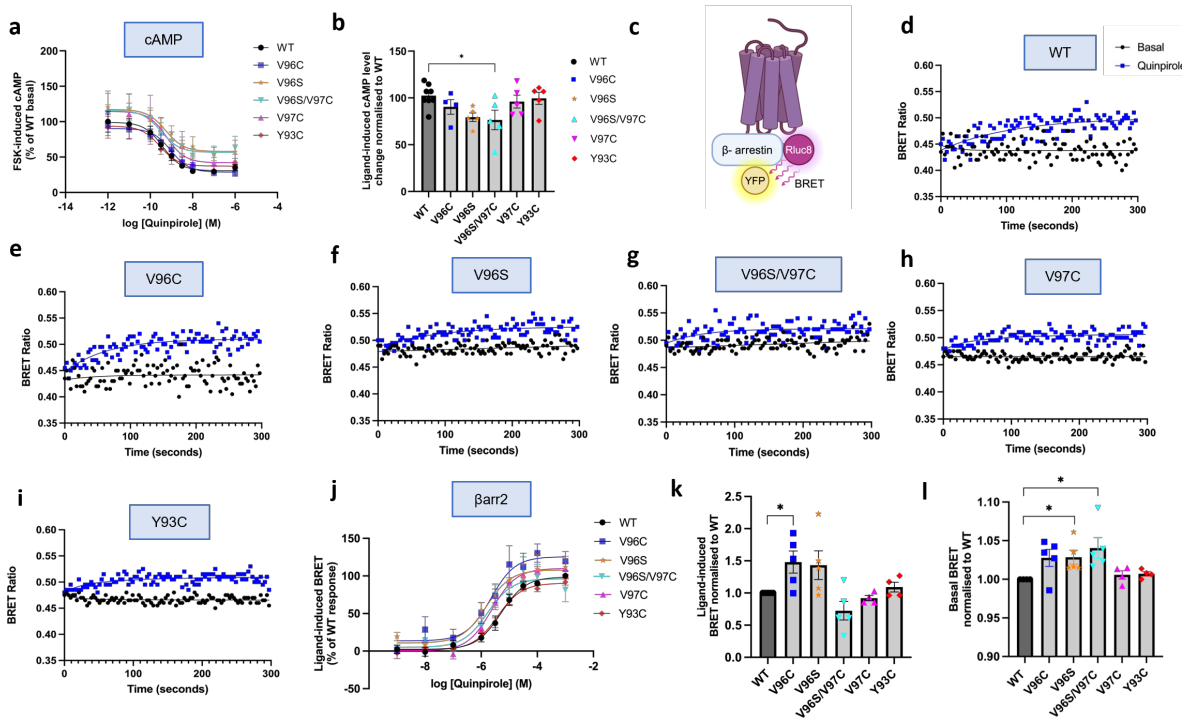

Fig. 3. Altered Gαi-signaling and βarr2 recruitment profiles of wildtype and mutant D_2R (a) Forskolin-induced cAMP levels as a percentage of basal cAMP levels of corresponding D_2R WT, quinpirole concentration response curves in D_2R WT (black) or mutant D_2R transfected HEK293 cells. Values plotted are +/- SEM of 4-5 independent experiments for D_2R mutants and 8 for WT. (**b**) Plot of quinpirole-induced cAMP levels, calculated as a change in cAMP levels in from cells treated with the maximum to the minimum dose of quinpirole, represented as a percentage of WT. One-way ANOVA and Dunnett's multiple comparisons test used to measure statistical differences between WT and mutant maximal responses (p*= 0.00282 (V96S/V97C)) (**c**) Schematic showing BRET assay. Representative kinetic curve showing BRET ratios in HEK293 cells expressing βarr2-YFP and D_2R WT (**d**), V96C (**e**), V96S (**f**), V96S/V97C (**g**), V97C (**h**), Y93C (**i**). Plotted over time for basal (black) and after 10 μM quinpirole stimulation (blue). Graphs representative of 4-6 independent experiments. (**j**) BRET luminescence values were measured before agonist addition and after addition of 1 nM – 1mM quinpirole, values are average of measurements taken over 5 minutes. Represented as a percentage of D_2R WT maximal response, for each individual experiment. (**k**) To determine the efficacy of quinpirole to induce βarr2 recruitment, for each individual experiment, ligand-induced BRET values were plotted for cells treated with the maximum dose of quinpirole (1 mM), represented as a fold change from D_2R WT. Basal BRET (**l**) of cells with no ligand and only PBS added prior to luminescence measurement for each individual experiment was plotted and presented as a fold change from WT. One sample t and Wilcoxon test. N=4 (V97C and Y93C) or 5 (V96C, V96S and V96S/V97C), +/- SEM. (p*= 0.0488 (k) or 0.0344 or 0.0398).

To assess the impact of these mutant D_2Rs on βarr1/2 recruitment, BRET assays were carried out in HEK293 cells expressing D_2R and βarr1/2. The kinetics of βarr1/2 recruitment were analysed in real time via BRET measured over a time-course of 5 minutes following agonist stimulation. The WT D_2R did not recruit βarr1 following

249 quinpirole treatment (Supplementary Fig. 7a and c). However, in cells expressing D_2R
250 WT and βarr2-YFP there was a rapid increase in BRET levels specifically after
251 quinpirole addition, up to a maximum level of BRET signal which remained stable for
252 at least 5 minutes (Fig. 3d and Supplementary Fig. 8). All D_2R mutants (except for
253 D_2R-Rluc8 V96S/V97C) showed a similar profile (Fig. 3e-i). The ability of D_2R to couple
254 to βarr2 over βarr1 is consistent with other studies[40,41]. Calculation of ligand-induced
255 BRET values and subsequent curve-fitting of the BRET profile allowed quantification
256 of the kinetics of βarr2 recruitment to WT and mutant D_2Rs (Table 2 and
257 Supplementary Fig. 8). There was no significant difference in the plateau of the fitted
258 kinetic profiles between WT or any mutant D_2R. However, the halftime of the D_2R
259 V96C kinetic curve was significantly lower than WT, suggesting that D_2R V96C
260 exhibits altered βarr2 recruitment.
261
262 To assess if the potency of quinpirole to induce βarr2 recruitment to mutant receptors
263 was altered, cells were treated with increasing concentrations of quinpirole (Fig. 3j-l).
264 D_2R V96C and V96S receptors, but not V97C or Y93C, exhibited a leftward shift in the
265 concentration-response curves, compared to WT with significantly lower EC_{50} values
266 (Table 1). This suggests that in cells expressing the V96C and V96S mutants,
267 quinpirole exhibits increased potency towards βarr2 recruitment. Additionally, there is
268 a significant increase in basal βarr2 recruitment in cells transfected with D_2R V96S
269 and V96S/V97C compared to D_2R WT (Fig. 3l). Combined with the reduced ligand-
270 induced BRET signal in kinetic assays (Fig. 3), this may suggest increased constitutive
271 association between the V96S/V97C receptor and βarr2. These signaling changes
272 were not due to alterations in cell surface receptor expression as reducing D_2R WT
273 cell surface expression to levels obtained with the mutant receptors had no impact on

274 the signal activity profile (Fig. 4 and Supplementary Fig. 9). Given that certain D_2R
275 mutants exhibit both stabilized/enhanced homomerization and a potential bias to
276 βarr2, we then assessed whether UNC9994, a D_2R-selective ligand, which has been
277 reported to show biased βarr2 signaling in some cell contexts, impacted D_2R WT
278 signaling and homomerization (Supplementary Fig. 10)[42,43]. A significant decrease in
279 D_2R-mediated Gαi signaling was observed and while a more transient kinetic profile
280 was observed for βarr2 recruitment, this was not enhanced compared to quinpirole,
281 suggesting UNC9994 acts as a partial biased agonist in this context. Additionally,
282 UNC9994 did not impact D_2R homomer associations as indicated by the BRETmax or
283 BRET50 values, similar to what was observed following quinpirole stimulation
284 (Supplementary Fig. 10 e-g).
285
286 Overall, this data suggests that V96C, and to some extent V96S show altered
287 quinpirole-induced βarr2 recruitment to D_2R, while V96S/V97C exhibits enhanced
288 constitutive association of βarr2. Furthermore, these receptors exhibit bias towards
289 βarr2 recruitment over Gαi signaling pathways.
290

291 **Constitutive and ligand-induced receptor internalization is enhanced**
292 **in D_2R V96S/V97C mutants**

293 β-arrestins play key roles in regulating GPCR signal activity[44,45]. One function is driving
294 receptor-mediated internalization. Given the faster (V96C) βarr2 recruitment and, in
295 particular, the ligand-independent (V96S/V97C) recruitment of βarr2, the cell surface
296 expression of these D_2Rs was assessed via flow cytometry and confocal microscopy.
297 While all receptors were shown to traffic to the membrane (Supplementary Fig. 11),
298 the cell surface expression of V96S/V97C was lower than WT D_2R (Fig. 4a). Due to
299 the observation that V96S/V97C also shows increased basal βarr2 recruitment, the
300 possibility that this decrease in cell surface expression was due to increased
301 internalization was investigated. The percentage of constitutively internalized receptor
302 was calculated as a percentage decrease of cell surface expression in cells incubated
303 at 37 °C following live antibody labelling, compared to cells incubated at 4°C to prevent
304 receptor internalization (Fig. 4b). Cells were gated to quantitate levels of D_2R in βarr2-
305 YFP-expressing cells. An increase in constitutive internalization of V96S/V97C
306 compared to WT receptor was observed, while Y93C had decreased internalization,
307 and all other mutants showed comparable levels of internalization to cells expressing
308 WT receptor. This increase in constitutive internalization may at least partially account
309 for the decrease in cell surface expression for D_2R V96S/V97C compared to WT.
310 There was a significant increase in ligand-induced internalization for all mutant
311 receptors, compared to WT and this increase was most dramatic in D_2R V96S/V97C-
312 expressing cells (Fig. 4c).
313
314 The altered ligand-induced and constitutive internalization in mutant D_2Rs observed
315 quantitatively by flow cytometry, was also confirmed by confocal microscopy (Fig. 4d).

316 Given the decrease in cell surface expression of some D_2R mutants, the impact of
317 lower cell surface D_2R expression on internalization and signaling was assessed.
318 Transfection of lower amounts of WT D_2R plasmid resulted in lower cell-surface
319 receptor expression, however, this decrease in WT expression did not cause a
320 significant change in ligand-induced or constitutive internalization or the efficacy of
321 quinpirole-mediated Gαi signaling (Supplementary Fig. 9c-e), suggesting increased
322 internalization and decreased Gαi signaling in receptor mutants is not solely due to
323 lower cell surface expression. Additionally, reduction WT D_2R expression to a
324 comparable level to the V96S/V97C receptor, results in the opposite effect of a
325 decrease in basal associations with βarr2, suggesting that the observed increase in
326 basal BRET associations with βarr2 in V96S/V97C-expressing cells compared to WT
327 is not solely due to lower expression levels of mutant receptor (Supplementary Fig. 9a
328 and b and Fig. 3). This data suggests that enhanced basal βarr2 association may
329 promote both ligand-independent and ligand-induced internalization.

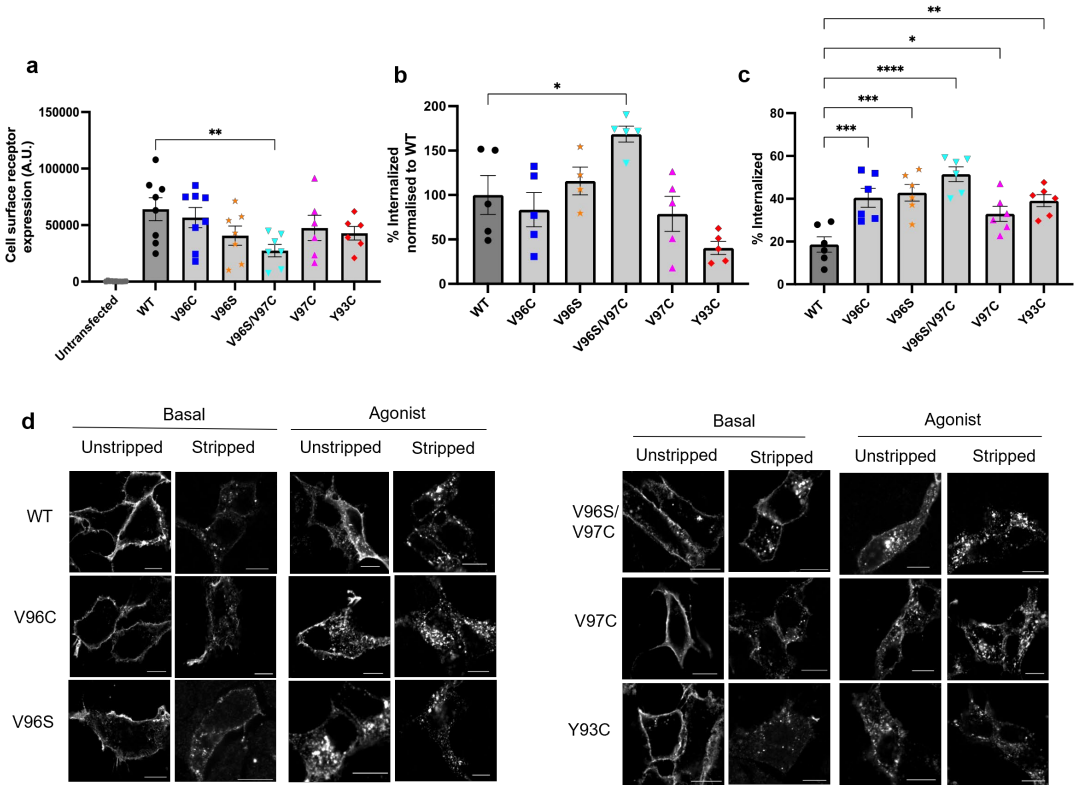

Fig. 4. Receptor cell surface expression and internalization assessed by flow cytometry and immunofluorescence microscopy. HEK293 cells transfected with D_2R constructs were labelled with M1 anti-FLAG primary and Alexa647 conjugated secondary antibody to quantify cell surface receptor expression. (**a**) Mean fluorescence and % of gated cells were multiplied to give a total value for cell surface D_2R expression. N=6-8. (**b**) In cells expressing βarr2-YFP, constitutive internalization of receptor constructs was calculated as a percentage change of cell surface receptor expression in cells incubated at 4°C to prevent receptor internalization, compared to cells incubated at 37°C following antibody labelling, which can continue to constitutively internalize receptor . Expressed as a percentage of WT for each individual experiment. N= 4 or 5. (**c**) Quinpirole-induced receptor internalization. Measured as a percentage decrease in cell surface expression level following 10 μM quinpirole stimulation, compared to untreated cells. N=6. In a-c, error bars are +/- SEM. One-way ANOVA followed by Dunnett's multiple comparison test used to measure statistical differences between WT and mutant D_2R (p*=0.0273 (b) or 0.0369 (c), p**= 0.0065 (a) or 0.0018 (c), p***<0.0009 or 0.0003, p**** <0.0001. (**d**) Representative confocal microscopy images showing D_2R localisation under basal conditions and after 30 minutes 10 μM quinpirole stimulation, with and without 'stripping' of cell surface bound anti-FLAG antibody. Representative of 3 independent experiments. Scale bar= 10 μm.

333 **D_2Rs that promote βarr2 recruitment favor βarr2-mediated ERK**
334 **signaling**

335 Arrestins play well-documented roles in mediating activation of extracellular signal-
336 regulated protein kinase (ERK) signaling[46], therefore, the impact of these mutations
337 on the phosphorylation levels of ERK1/2 was assessed. D_2Rs WT, V96S and
338 V96S/V97C increased ERK activation up to a maximal level following 2-5 minute
339 stimulation with quinpirole (Fig. 5a and b). However, V96C exhibited enhanced
340 agonist-dependent ERK signaling compared to WT at the 5-minute quinpirole
341 stimulation timepoint, while V96S/V97C exhibited a more rapid ERK signaling profile
342 (Fig. 5a and b). In CRISPR βarr1/2 knockout-cells, the ability of WT D_2R to increase
343 phospho-ERK levels after quinpirole stimulation was maintained (Fig. 5c-e). D_2R
344 V96C, V96S and V96S/V97C, however, exhibited a decrease in agonist-dependent
345 ERK signaling (Fig. 5f-h and Supplementary Fig. 12). This sensitivity/requirement of
346 βarr for ERK signaling could be due to the altered βarr2 association profiles of these
347 D_2R mutants, which also in turn exhibit enhanced/stabilized homomer associations.
348

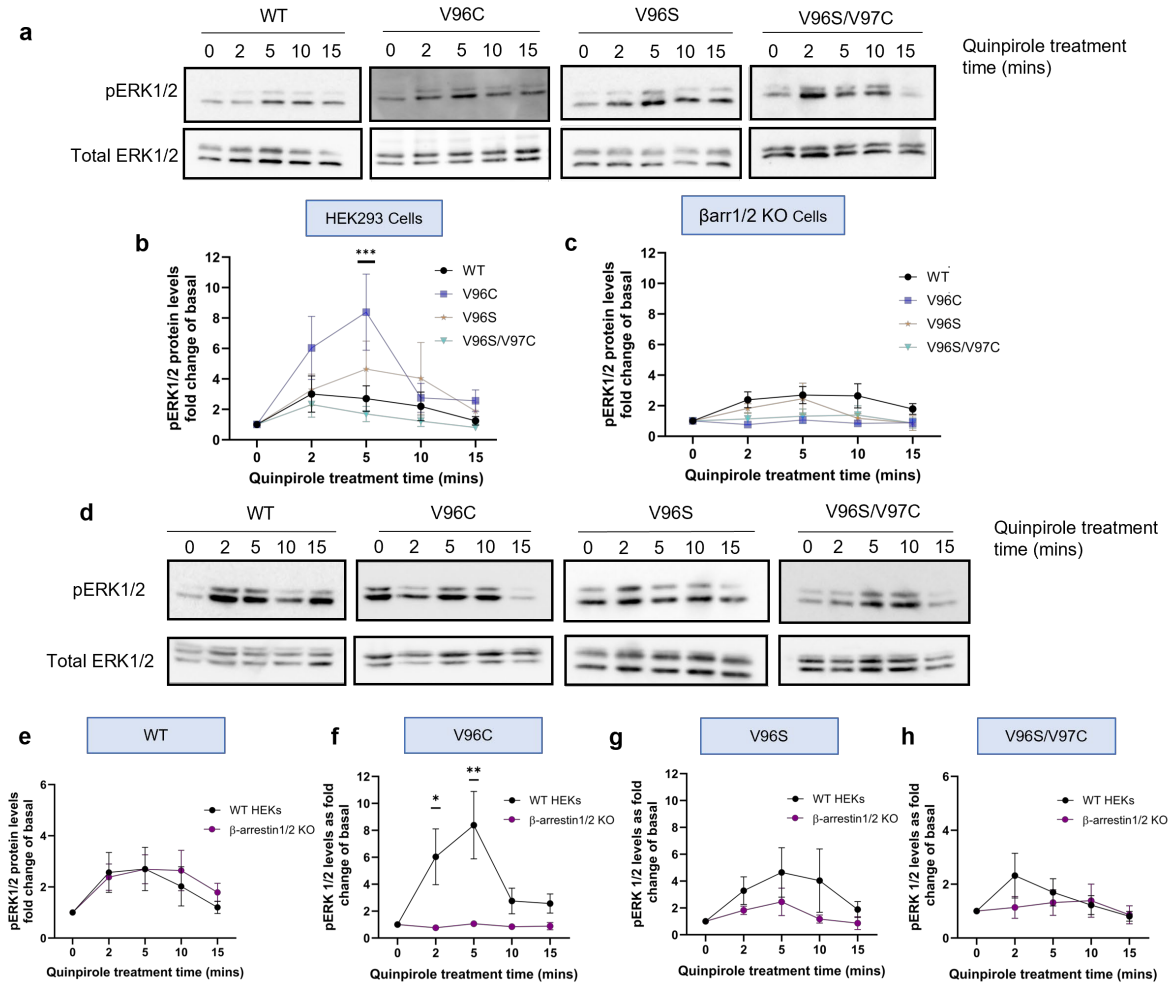

Fig. 5. Ligand induced ERK1/2 activation in HEK293 cells and βarr 1/2 knockout cells. Representative Western blots on HEK293 cells (**a** and **b**) or HEK293 βarr 1/2 KO (βarr 1/2 KO) cell lysates (**c** and **d**) transfected with D_2R constructs and treated with 10 μM quinpirole for 2, 5, 10 or 15 minutes, probed with phospho-ERK 1/2 and total ERK 1/2 antibodies. Normalised ligand-induced phospho-ERK 1/2 levels expressed as a fold change of basal levels quantified in HEK293 (**b**), or βarr 1/2 KO cell lysates (**c**) transfected with D_2R-Rluc8 WT (black) vs V96C (blue), V96S (orange), V96S/V97C (turquoise) constructs. (**e-h**) Direct comparison of relative pERK1/2 levels in WT HEK293 (black) or βarr 1/2 KO cells (purple) transfected with D_2R WT (**e**), V96C (**f**), V96S (**g**), V96S/V97C (**h**) . Mean +/- SEM, N=5 (V96S and V96S/V97C) or 6 (V96C) for mutant receptors in HEK293 cells and 4 (V96C and V96S/V97C) or 5 (V96S) in βarr 1/2 KO cells and N=8 for WT D_2R. Two-way ANOVA followed by Šídák's multiple comparisons test used to measure statistical differences between WT and mutant D_2R (in b p***<0.0005, in f p*= 0.0439 and p**=0.015).

349

350 **Differential stoichiometry of D_2R dimers with its G proteins or arrestin**

351 Insights into the architecture of the assemblies between dimeric D_2R and
352 heterotrimeric Gαi or βarr2 were inferred from molecular modelling. By fitting the D_2R
353 from the cryoEM structure in complex with heterotrimeric Gαi (PDB: 8IRS) onto both
354 protomers in each of the predicted D_2R homodimers, a 2:1 D_2R:Gαi stoichiometry is
355 predicted (Supplementary Fig. 13). Steric clashes occur between two G-protein
356 heterotrimers simultaneously docked to the D_2R homodimer, making a 2:2
357 stoichiometry unlikely. This suggests that for dimeric D_2R the proper D_2R:Gαi
358 stoichiometry is 2:1 and any stabilization at the H1-H2 D_2R homodimer, especially
359 V96S/V97C, is expected to reduce the number of receptors available for binding to
360 heterotrimeric Gαi, thus reducing coupling efficiency. The 2:1 D_2R:Gαi stoichiometry
361 is in line with the minimal signaling unit found to maximally be activated by agonist
362 binding to a single protomer in an asymmetrical activated D_2R dimer [47] .
363
364 Docking simulations between the homodimers of D_2R WT, V96C, and V96S/V97C and
365 two different structural models of βarr2 always predicted receptor-arrestin complexes
366 similar to the cryoEM complexes (see Methods). It is worth noting that in all dimeric
367 complexes, the D_2R is in an active state as it was extracted from the cryoEM complex
368 with the agonist ritigotine and heterotrimeric Gi (PDB: 8IRS). Remarkably, the
369 architecture of the H1-H2 D_2R dimers favors the simultaneous recruitment of two βarr2
370 molecules (i.e. with a D_2R:βarr2 2:2 stoichiometry) (Fig. 6a and b). Noticeably, the
371 finger loop holds a different conformation in the two βarr2 models, which was inherited
372 from the two different βarr1 structural templates, the finger loop being unstructured in
373 6TKO while holding one α-helical turn in 7SRS. In the predicted complexes between
374 WT or mutant D_2R dimers and both βarr2 structural models, the central-crest loops of

375 active βarr2 form a docking site for IL2 of the receptor, which holds a two-turn α-helix.
376 Specifically, the finger loop of βarr2 docks in the receptor site contributed by the
377 cytosolic extensions of H3 and H6 as well as IL1, IL2, and H8. Furthermore, the middle
378 loop and the β-hairpin that includes the C-loop of βarr2 make contacts with IL2 and
379 H5 of the receptor (Fig. 6a and b). While the interface described above is common to
380 all prototypical GPCRs, an additional interface between the N-terminal domain of βarr2
381 and the phosphorylated tail of the receptor is formed only when such tail is present,
382 which is not the case of D_2R.[48] Lack of the phosphorylated C-tail may have an effect
383 on the process of βarr-receptor recognition but not on the final architecture of the
384 complex, which is expected to be the same independent of the presence or absence
385 of the C-tail. Therefore, the D_2R dimer-stabilizing mutants both reduce the number of
386 receptors available for Gαi coupling, whilst favoring βarr2 coupling. Measurement of
387 D_2R homomer interactions via BRET saturation assays in βarr½2 KO cells suggested
388 that the lack of βarr1/2 did not significantly alter D_2R dimerization (Supplementary Fig.
389 14). This may suggest that D_2R dimers form distinct conformations in the presence or
390 absence of βarrs, without changing overall dimer stability.

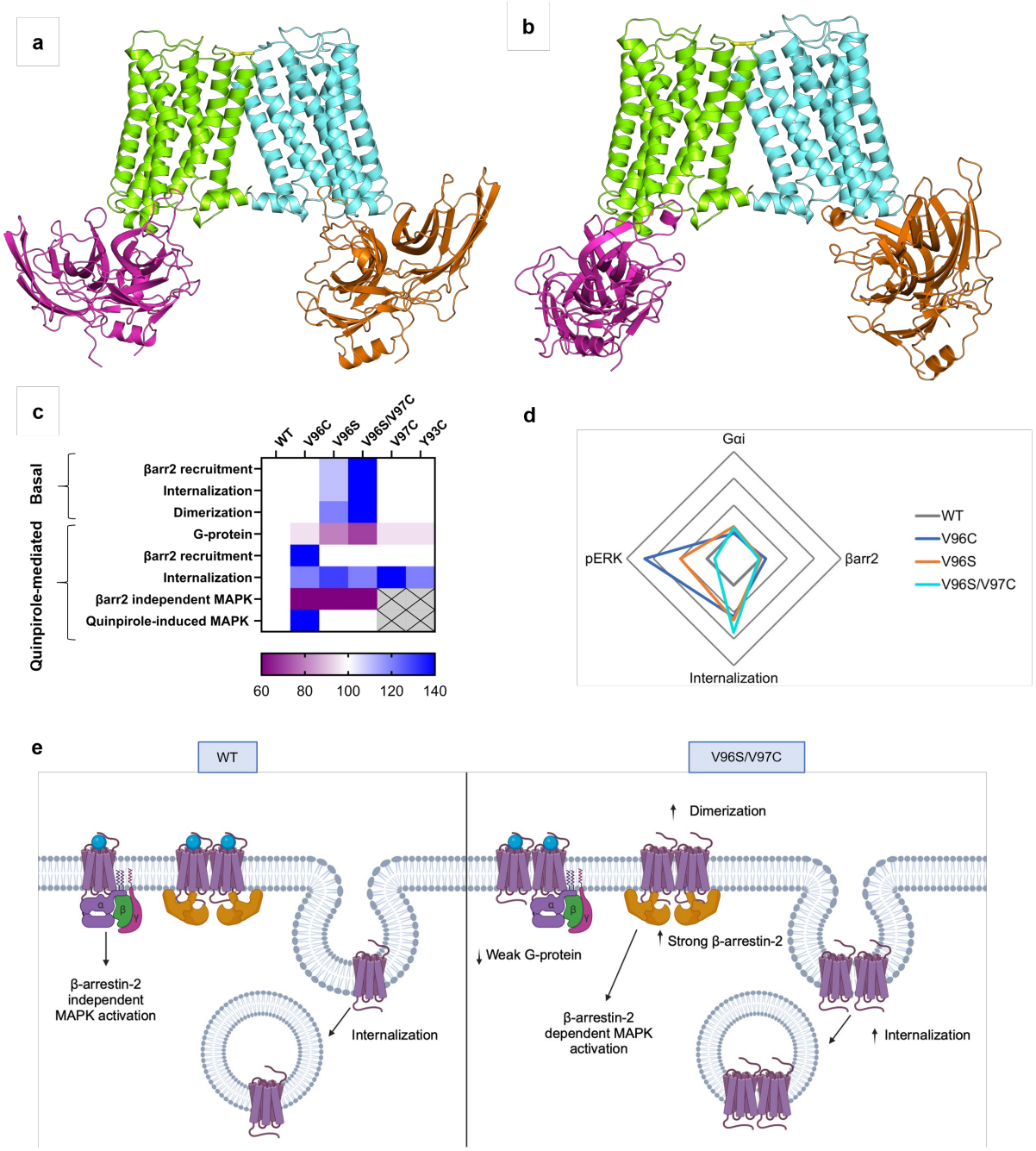

Fig. 6. Predicted models for D_2R homodimer-βarr2 complexes and summary schematics. The cartoon representations of two different structural complexes between the V96S/V97C mutant D_2R homodimer (protomers lemon-green and aquamarine) and βarr2 (orange and magenta) are shown. The structural models of βarr2 shown in the **a** and **b** panels have been, respectively, achieved by using the βarr1 structures from the 6TKO and 7SRS cryoEM complexes as templates. The side chains of C97 are shown in yellow sticks; the distance between the two sulfur atoms is 2.0 Å. I) Heat map summarising the functional effects

399 of D_2R mutants relative to WT. 100 is WT and white, an increase relative to WT is blue and a
400 decrease is purple. (**d**) Quinpirole induced Gi signalling, βarr2 recruitment, quinpirole-induced
401 internalization and pERK activation of D_2R mutants as a fold change relative to D_2R WT. G-
402 protein and β-arrestin bias calculated as Emax/EC_{50} (**e**) Summary schematic of proposed
403 βarr2 biased signalling from D_2R V96S/V97C oligomers.

404 **DISCUSSION**

405 Combining molecular docking simulations with biophysical, super-resolution and
406 functional studies, we propose a model for stabilizing D_2R homomer associations and
407 demonstrate the utility of such an approach to identify a mechanism for not only
408 stabilizing receptor-receptor associations, but also for promoting both βarr2 interaction
409 and βarr2-mediated functions. This reveals a potential role for D_2R di/oligomerization
410 in βarr2-biased signaling that could be targeted for therapeutic benefits.

411

412 The predicted interface in symmetric D_2R homodimers with both protomers either
413 inactive or active, characterised by H1-H1, H1-H2, and H2-H2 contacts (i.e. H1,H2
414 dimer), is shared with other published high-resolution GPCR dimer structures including
415 rhodopsin, κ-opioid, β1-adrenergic, μ-opioid, and human apelin receptors[49–53].
416 Previous studies have suggested that H4 participates in D_2R homodimer interface, but
417 a second interface involving H1 and H8 has also been suggested[28,54,55]. We found the
418 involvement of H4 in some D_2R dimers with both protomers inactive or with asymmetric
419 inactive-active dimers, though with worse membrane topology. Additionally, several
420 studies have suggested that IL1, EL2 and EL3 are important in stabilizing GPCR dimer
421 interactions[55–57]. However, this is based on computational modelling and biophysical
422 data, with no current published dimer structure for the D_2R homodimer. It is also
423 possible that multiple dimer interfaces exist, as reported for the β1AR, where both a
424 H1-H2-H8-EL1 and H4-H5-EL2-IL2 interfaces exist[49]. Given we observed both dimers
425 and higher-order oligomers, we cannot rule out that D_2R interacts through additional
426 interfaces depending on whether it exists in a dimeric or higher-order complex.
427 Mutations at specific sites of the interface predicted herein increased the stability of
428 D_2R homomers, with the V96S/V97C double mutant exhibiting the greatest shift

429 towards D_2Rs in an oligomeric state in the absence of ligand (~6% increase in all
430 oligomer types compared to D_2R WT), indicating an increase in constitutive oligomer
431 stability. Super-resolution, single molecule analysis revealed there was little change in
432 the proportion of WT and V96S/V97C D_2Rs in an oligomeric state after cells were
433 stimulated with quinpirole. Interestingly, the proportion of V96S receptors in an
434 oligomeric complex at the cell surface were reduced when stimulated with quinpirole,
435 which could reflect that di/oligomers of this D_2R are internalized, consistent with the
436 enhanced ligand-induced internalization and oligomerization favouring βarr2 coupling.
437
438 Ligand bias, whereby ligands can promote one pathway over another, are of interest
439 both therapeutically and for understanding the molecular basis of pathway preferences
440 for different GPCRs, in different conformational states[58,59]. In this study, receptor
441 mutants, which showed increased di/oligomerization also showed increased ligand-
442 induced (V96C and V96S) or constitutive (V96S/V97C) associations with βarr2
443 (Summarised in Fig. 6c-e). It is important to note that while the BRET assay results
444 presented here suggest a steady state recruitment of βarr2, it cannot be ruled out that
445 this represents multiple GPCR-βarr2 associations and dissociations, perhaps with
446 distinct D_2R-βarr2 conformations[60].
447
448 There are many factors that can impact the signaling pathway preference of a GPCR,
449 including membrane lipid composition and localisation of receptors[35,61–64].
450 Interestingly, these factors have also been shown to influence oligomerization of
451 GPCRs[65]. While changes in the organisation of D_2R complexes at the cell surface
452 detected in PD-PALM experiments may be small, even slight changes in complex
453 formation can have dramatic effects on receptor signaling in cells[37,38]. By enhancing

454 specific receptor conformations such as a propensity to oligomerise and associate with
455 βarr2, the role of such conformations on receptor activity may be amplified. These
456 changes are in line with prior studies that have employed PD-PALM to assess GPCR
457 di/oligomerization, where even small changes in protomer composition within a single
458 oligomeric complex can direct how these receptors modulate signaling[37,38].
459
460 There is some debate about the role of βarrs in D_2R-mediated ERK activation. It is
461 likely that mechanisms are both cell-type specific and D_2R-isoform specific, with D_2R
462 long and short differing in the way they mediate MAPK activation[66,67]. Interestingly, the
463 apparent bias towards βarr2 recruitment in D_2R mutants results in enhanced
464 internalization a βarr2-dependent mechanism for downstream mediation of the MAPK
465 pathway. It is possible that increased dimerization of these mutants makes them more
466 likely to internalize as has been demonstrated from CXCR4 oligomers[19]. Taken
467 together, the most striking changes in signaling under basal conditions are observed
468 with the D_2R V96S/V97C double mutant which shows a strong preference for βarr2,
469 required for downstream signaling. Here we have shown that different D_2R mutants
470 exhibit distinct βarr2 signaling profiles, supporting the broad spectrum of GPCR-βarr
471 conformations that are being uncovered[68].
472
473 The impact of oligomerization on biased signaling has focused on heteromers rather
474 than homomers, including the $A_{2A}R$-D_2R heteromer[69,70]. Previous studies have
475 reported that oligomerization can either increase or decrease G-protein activation,
476 suggesting there is no consensus for all GPCRs in one class, but such behaviour is
477 receptor specific[19,21,71,72]. The role of GPCR oligomerization on βarr recruitment has
478 been less well studied. Oligomerization of the PAFR has been shown to cause a bias

479 away from βarr recruitment, while our study demonstrates an opposing role for the
480 D_2R[21] . It has been suggested that allosteric interactions between receptor protomers
481 upon receptor activation of the $A_{2A}R$-D_2R heteromer, causes the D_2R protomer to
482 favour βarr2 recruitment[70]. It is possible that a similar phenomenon is occurring in the
483 D_2R mutants explored in this study that exhibit increased βarr2 recruitment and
484 associated signaling, also exhibit enhanced homomer stability.
485
486 Dimerization has been suggested to significantly increase the surface area available
487 for arrestins to bind, which may provide a rationale for the increased oligomerization,
488 which we observe in receptor mutants that also show a bias towards arrestin-
489 mediated signaling pathways[11,73]. Consistently, the predicted D_2R dimer is able to
490 simultaneously accommodate two βarr2 molecules. It is possible that the V96S/V97C
491 double mutant and, to some extent, the V96S D_2R mutant, are showing a more 'active-
492 like' conformation in the absence of agonists, which causes them to associate more
493 readily with βarr2, causing increased internalization and a dependence upon βarr2 for
494 MAPK signaling. Previous studies have found that βarrs are involved in D_2R-mediated
495 ERK phosphorylation in the $A_{2A}R$-D_2R heteromer, but not when D_2R is expressed
496 alone[74]. It is also possible that for these D_2R mutants, increased homo-oligomerization
497 induces increased dependence upon βarr2 for signaling pathways. This is supported
498 by docking simulations between D_2R homodimers and βarr2, which showed a 2:2
499 receptor: βarr2 stoichiometry while showing a 2:1 receptor: Gi stoichiometry (Fig. 6a
500 and b and Supplementary Fig. 13). This suggests that D_2R dimers, and therefore
501 mutations which stabilize homo-di/oligomers, favour βarr2 coupling over Gi coupling.
502 These docking simulations may provide an insight into the structural basis behind the

503 observed increase in oligomerization in D_2R mutants that also exhibit increased βarr2
504 associations.
505
506 In conclusion, the role of D_2R oligomers in disease makes these complexes attractive
507 therapeutic targets[30,75–77]. The lack of high-resolution structures of the D_2R homodimer
508 has hindered our ability to exploit oligomers for therapeutic benefits. Here we suggest
509 models for the D_2R homodimer and experimental validation confirms a key role for H1
510 and H2 at the predicted D_2R homodimer interface to increase dimer stability, and a
511 bias towards βarr2. These mutant constructs could form the basis for structural studies
512 capturing D_2R homomers and specific D_2R- βarr complexes. More broadly, this study
513 provides a framework for engineering the stabilization of class A GPCR dimers and
514 may suggest that D_2R oligomers favour an 'active-like' conformation that promotes
515 βarr recruitment.

516 # METHODS

517 ## Molecular modelling

518 Prediction of likely architectures of D_2R homodimers relied on a computational
519 approach developed for quaternary structure predictions of transmembrane α-helical
520 proteins, including a number of GPCRs, i.e. FiPD-based approach[78–80]. It consists of
521 rigid-body docking using both a version of the ZDOCK program devoid of desolvation
522 as a component of the docking score (v2.1)[81] , followed by employment of a membrane
523 topology filter by the FiPD software to minimize false positives. A rotational sampling
524 interval of 6° was set (i.e., dense sampling) and the best 4000 solutions were retained
525 and ranked according to the ZDOCK score. Such solutions were then filtered
526 according to the "membrane topology" filter, which discards all those solutions that
527 violate the membrane topology requirements. The membrane topology filter, indeed,
528 discards all the solutions characterized by a deviation angle from the original z-axis,
529 i.e. tilt angle, and a displacement of the geometrical center along the z-axis, i.e. z-
530 offset, above defined threshold values, which were 0.4 radians and 6.0 Å respectively.
531 The filtered solutions underwent cluster analysis by using a 3-Å Cα-atom Root Mean
532 Square Deviation (RMSD) followed by visual inspection of the cluster centers for
533 selecting the final solutions on the basis of membrane topology indices and docking
534 score. Symmetrical D_2R homodimers holding both protomers either inactive or active
535 and asymmetric inactive-active dimers were predicted. The following structures were
536 probed as sources of D_2R protomers: a) inactive-state structures: 6CM4, 6LUQ, and
537 7DFP (i.e. D_2R in complex with risperidone, haloperidol, and spiperone, respectively),
538 and b) active-state structures: 7JVR and 8IRS (i.e. the ternary complexes between
539 heterotrimeric Gi and D_2R in complex with bromocriptine and ritigotine, respectively).
540 The best results in terms of reliable docking solutions (according to the membrane

541 topology indices) were achieved, for the active-state dimers, by using D_2R from 8IRS
542 as a protomer, and, for the inactive-state dimers, by-using D_2R from 6CM4 completed
543 with the missing IL2 as a protomer. . The employment of an active-state structural
544 model of D_2R was also instrumental in predicting supramolecular complexes between
545 D_2R dimers and either βarr1 or βarr2. The latter predictions were carried out by
546 ZDOCK v3.0.2[82] coupled with a FiPD-based filtering approach based on a distance
547 cutoff between the DRY arginine (R132) of D_2R and L/V71 in the finger loops of βarr1
548 or βarr2, respectively, followed by cluster analysis. In those docking simulations, the
549 receptor was used as a fixed target while βarr1 or βarr2 was used as a probe. The
550 structural model of receptor-bound βarr2 were achieved by comparative modelling (by
551 Modeller[83]), using the cyoEM structures of βarr1 bound either to the β_1-AR (PDB:
552 6TKO) or to the $5HT_{2B}$ receptor (PDB: 7SRS) as templates. Remarkably, the two βarr1
553 templates differed in the conformation of several loops including the finger loop, an
554 essential recognition point for receptor binding. Such comparative modelling was
555 necessary because none of the available βarr2 structures, co-crystallized with
556 peptides from the C-tails of a number of GPCRs, represent real receptor-bound forms
557 as far as conformation and arrangements of the loops in the central crest are
558 concerned. Accordingly, the employment of those βarr2 structures in docking
559 simulations with the D_2R did not produce any reliable solution. The employment of
560 two different structural models of βarr2 served to overcome in part the lack of cryoEM
561 complexes of βarr2 with GPCRs and to take into account possible structural variability
562 in the receptor-bound states of the same arrestin. For βarr1, the most complete
563 versions of the cryoEM structures 6TKO and 7SRS were employed. Only the results
564 of βarr2-D_2R docking are shown here. Evaluation of the native-like feature of a docking

565 solution was based on structural comparisons with the cryoEM receptor-βarr1
566 complexes (6TKO and 7SRS).
567

568 **Cell Culture and transfection**

569 HEK293 cells (human embryonic kidney cells) and βarr1/2 knockout cells were
570 maintained as a monolayer in T-75 cm2 flasks (Sigma). βarr1/2 knockout HEK293
571 cells were made by using CRISPR-Cas9 (kindly provided by Asuka Inoue, Univ.
572 Tohoku). Cells were cultured in Dulbecco's Modified Eagle's Medium (DMEM) media
573 (Gibco) containing 4.5 g/L glucose, 1% (v/v) L-glutamine and supplemented with 10%
574 (v/v) FBS (Gibco), 1% (v/v) streptomycin/penicillin (Sigma) in a humidified atmosphere
575 of 5% CO_2 at 37°C. Cells were usually passaged every 3-4 days in a 1:10 ratio using
576 0.05% (v/v) trypsin (Gibco, UK) in phosphate buffered saline (PBS). HEK293 cells
577 were seeded and cultured in 6 well plates 1 day before transfection in DMEM with 10%
578 (v/v) FBS (Gibco), 1% (v/v) streptomycin/penicillin (Sigma). Cells were transfected at
579 80-90% confluency with Lipofectamine 2000 reagent (Invitrogen, UK).
580

581 **Plasmid DNA constructs**

582 βarr1-YFP and βarr2-YFP plasmids were obtained from Frederic Jean-Alphonse
583 (CNRS, Nouzilly). FLAG-D_2R-Venus and Rluc8 plasmids were obtained from
584 Jonathan Javitch. The FLAG-D_2R-Rluc8 plasmid was used to obtain the D_2R Cys
585 mutant constructs using the Agilent Quikchange II site-directed Mutagenesis Kit
586 according to the manufacturer's instructions. Mutant D_2R constructs were introduced
587 into D_2R-Venus plasmids via the In-Fusion Snap Assembly cloning kit (Takara)
588 according to manufactures instructions and inserted into FLAG-D_2R-Venus DNA using

589 BamHI and Kpn1 restriction sites. See Supplementary table 2 for a list of plasmids
590 used in this study.
591
592 **BRET saturation assays**

593 Cells were transfected with constant amounts of D_2R-Rluc8 plasmid DNA and
594 increasing amounts of D_2R-Venus (0-3 µg in 6 well plates) plasmid and assayed 48
595 hours post-transfection. Cells in suspension were plated in white 96 well plates in
596 triplicate. Coelenterazine-h (Promega) was used at a final concentration of 5 µM.
597 BRET emissions using the short-wavelength filter at 475 nm and long wavelength filter
598 535 nm were measured in 10 repeat cycles using a LUMIstarOPTIMA plate reader
599 (BMG Labtech). Fluorescence of Venus-tagged receptor was measured in duplicate
600 after excitation at 485 nm and emission at 535 nm.
601
602 For each condition, net BRET values were calculated (535 nm value/ 475 nm value)
603 over 10 cycles, where BRET ratios for the negative control donor only condition were
604 subtracted. Rluc8 values (475 nm emission value) were averaged over the 10 cycles
605 and again for the duplicate repeats. Net Venus values were calculated by subtracting
606 Venus measurements of donor only conditions. Net BRET values were plotted against
607 Net Venus/Rluc8 using GraphPad Prism 10 and fitted with a non-linear binding curve
608 assuming one site-specific binding.
609
610 **β-arr recruitment BRET assays**

611 HEK293 cells were transfected with D_2R-Rluc8 plasmids and βarr1/2-YFP constructs.
612 48 hours post transfection cells were resuspended in PBS. For BRET time course
613 assays, Venus expression (excitation 485 and emission 535 nm) was measured. For

614 basal BRET emissions, a separate set of duplicate cell suspensions were measured
615 at 475 nm excitation and 535 nm emission wavelengths after addition of 5 μM
616 coelenterazine-h (Promega). PBS or 10 μM quinpirole was added to cell suspensions
617 and BRET emissions were immediately measured again. Raw BRET ratios were
618 calculated (535 nm value/ 475 nm value). To calculate ligand induced BRET, basal
619 BRET ratios were subtracted from BRET ratios after agonist addition. For dose
620 response BRET experiments, increasing concentrations of quinpirole agonist was
621 added to sets of duplicate cell suspensions after basal BRET emissions had been
622 measured. After ligand induced BRET values had been calculated, data was
623 normalised by subtracting the control with only PBS added.
624
625 Analysis was based on βarr recruitment waveform methods as previously described
626 [84]. The BRET emissions were measured every 3-5 seconds for a total of 5 minutes.
627 Ligand-induced BRET ratios were calculated and plotted against time and recruitment
628 of βarr was observed to be stable recruitment, where the waveform rises to a steady
629 state. The waveforms were fitted to non-linear one-phase association curve in
630 GraphPad Prism 10 to allow quantification of kinetics. The rate constant s-1 was
631 quantified and can be represented as the halftime, in seconds, (computed as ln(2)/k).
632 The steady-state level of recruitment is represented as the plateau of the waveform,
633 which also indicates the affinity of the receptor for βarr. The initial rate of recruitment
634 was also calculated as k*span (maximum BRET ratio).
635
636 **Flow cytometry**
637 Cells were live labelled with M1 anti-FLAG antibody (1:1000 Sigma Aldrich, no.3040)
638 48 hours post transfection for 30 minutes at 37 °C. For the flow internalization assay,

639 antibody incubation was carried out at 4°C for 1 hour for all cells, then one set of cells
640 were transferred to the 37 °C incubator and allowed to recover for 1 hour. Agonist
641 stimulation at 37°C was carried out 30 minutes in to the 1-hour recovery period. The
642 other set of cells was kept at 4 °C and washed 3 times with cold DMEM media. Cells
643 were resuspended in FACS buffer (PBS with $Ca^{2+}$and Mg^{2+} and 2% FBS), centrifuged
644 and the cells resuspended in either FACS buffer alone for untreated cells or with Alexa
645 Fluor 647 antibody (1:2000; Invitrogen, A32728). Cell suspensions were incubated for
646 1 hour on ice and washed in FACS buffer three times. The cell suspensions were
647 transferred to individual round bottomed polypropylene tubes and the
648 immunofluorescence measured on a FACS Calibur Flow Cytometer (BD biosciences).
649

650 **cAMP assay**

651 HEK293 were transfected with 1 µg of D_2R-Rluc8 constructs. After 24 hours,
652 approximately 40,000 cells/well were replated into a 96-well format in triplicate for each
653 condition. After a further 24 hours, the cells washed with PBS and pre-treated with 0.5
654 mM IBMX in DMEM with 0.1% Bovine serum albumin (BSA) for 5 minutes at 37°C.
655 Forskolin was diluted in 0.5mM IBMX in DMEM 0.1% BSA to give a final concentration
656 of 3 µM. Cells were stimulated with ligands diluted in the forskolin solution and
657 incubated at 37°C. After stimulation, cells were washed with ice cold PBS and lysed.
658 The level of cAMP in lysates was measured using the cAMP Gs Dynamic 2 kit
659 (Revvity).

660

661 **Western blotting**

662 Cells were washed with PBS and lysed with ice cold RIPA lysis buffer (50 mM Tris
663 pH7.4, 1% Triton X-100, 140 mM NaCl, 5 mM EDTA, 1 mM NaF, 1 mM PMSF, 1 mM
664 sodium orthovandate and a protease inhibitor tablet (Roche)). Protein concentrations
665 were determined using BSA standard curve and diluted in Laemmli sample buffer
666 (Sigma) in the presence or absence of 5% 2-β-mercaptoethanol. Samples were
667 separated via SDS-polyacrylamide gel and transferred to a nitrocellulose membrane.
668 The membrane was blocked and incubated in primary antibody diluted overnight (See
669 Supplementary Table 1). Membranes were incubated in HRP-linked secondary
670 antibody and imaged using Immobilon Forte Western HRP reagent (Millipore) and X-
671 ray film (Amersham) or Chemi-imager. The band intensities were analysed using
672 Image J.

673

674 For pERK Western blotting, cells were serum starved for 16 hours before quinpirole
675 stimulation and lysis of cells. All lysates were diluted to 20 µg of protein in Laemmli
676 buffer in the presence of 5% 2-β-mercaptoethanol, boiled for 5 minutes at 95°C before
677 loading. Quantification of protein intensity was done separately for each blot and
678 where multiple blots were used the same D_2R WT lysates were employed to allow
679 direct comparison with mutant D_2R on the same membrane.
680

681 **Confocal Microscopy**

682 Transfected cells were replated onto coverslips in a 24 well format with approximately
683 75,000 cells/well and left for a further 24-48 hours. Cells were incubated in M1 anti-
684 FLAG antibody (Sigma Aldrich, no.3040) diluted 1:500 with or without 10 µM quinpirole
685 for 30 minutes at 37°C. To remove the cell surface antibody, cells were washed 3
686 times with 0.04 M EDTA in PBS-Ca^{2+} before fixation. Cells were then fixed with 4%
687 PFA in PBS-Ca^{2+}, permeabilised with 0.2% Triton-X in PBS-Ca^{2+} and blocked for 1
688 hour at RT in 2% FBS in PBS-Ca^{2+}prior to incubation in Alexa Fluro-conjugated
689 secondary antibody (1:000 dilution) (Thermofisher, A32728). Slides were mounted
690 onto coverslips and imaged were obtained with a Leica Stellaris 8 microscope using a
691 64 x oil immersion objective and sequential excitation at wavelengths of 405, 488 and
692 647 nm.
693

694 **PD-PALM**

695 Transfected cells were plated onto 35mm dishes (Mattek) with 14mm x 1.5mm glass
696 coverslips. Anti-FLAG (Sigma Aldrich) primary antibodies were labelled with photo
697 switchable dye CAGE 500 according to the manufacturer's instructions to give a 1:1
698 antibody:dye molar ratio (Abberior). Live cells were incubated with FLAG-CAGE500
699 conjugated antibody, diluted in 10% FCS in PBS Ca2+, at 37 °C for 30 minutes. All
700 steps from antibody addition to imaging were carried out in the dark to prevent
701 activation on the conjugated antibodies. Cells were washed in PBS Ca2+ before
702 fixation in 4% PFA and 0.2% Glutaraldehyde for 30 minutes (Sigma) and maintained
703 in PBS Ca^{2+}.

704

705 PALM images were acquired using the Zeiss Eyra PS1 microscope with 1.45
706 numerical aperture, 100x oil immersion objective in total internal reflection
707 fluorescence (TIRF) mode. Photoactivation of CAGE 500 dye was achieved by
708 simultaneous activation with 405 nm (UV light) and excitation and photobleaching with
709 488 nm laser. Lasers were switched on 30 minutes before imaging to allow
710 stabilization. Images were captured over 20,000 frames with an exposure time of 100
711 ms using the ZEN software.

712

713 Location analysis of receptors was done using the QuickPALM plugin in Fiji, as
714 previously described [85]. Two 7x7 µm region of interests were analysed within the cell
715 boundary using the QuickPALM plugin. The parameters used were typically a signal
716 to noise ratio of 7 and a full-half width maximum of 5, although these were determined
717 for each experiment. This analysis outputs XY coordinates of the localised particles
718 with sub-pixel accuracy. Particles within 20 nm of each other were discounted to

719 prevent overestimation of receptor complexes. The coordinates were inputted into a
720 Java- based PD-interpreter application [38,39]. to determine the number of associated
721 receptor molecules. This app uses Getis-Franklin neighbourhood analysis with a
722 search radius of 50 nm. The software discounts a receptor from further searches once
723 it has been assigned as participating in a homomer, to prevent double counting. The
724 output is a table containing both the number of associations and the number of
725 receptor molecules in each complex.

726 **Quantification and statistical analysis**

727 All statistical analysis was performed in GraphPad Prism 10. Specific statistical tests
728 are noted in each figure legend. In most cases, two-tailed, unpaired t-tests was used
729 when comparing two groups or one-way ANOVA with Dunnett's multiple comparison
730 test was used for multiple groups. For comparing two variables and multiple groups,
731 two-way ANOVA followed by Šídák's multiple comparisons test was used. In all tests,
732 $p<0.05$ was considered statistically significant.

733

DATA AVAILABILITY

Source data are provided with this paper. Any additional data that support the findings of this study are available from the corresponding author upon reasonable request.

CODE AVAILABILITY

Custom codes used to analyse PD-PALM data are provided as an attached Zip file.

740 ## References

741 1. Syrovatkina, V., Alegre, K. O., Dey, R. & Huang, X.-Y. Regulation, Signaling,
742 and Physiological Functions of G-Proteins. *J Mol Biol* **428**, 3850–3868 (2016).
743 2. Hauser, A. S., Attwood, M. M., Rask-Andersen, M., Schiöth, H. B. & Gloriam, D.
744 E. Trends in GPCR drug discovery: new agents, targets and indications. *Nat Rev*
745 *Drug Discov* **16**, 829–842 (2017).
746 3. Yang, D. *et al.* G protein-coupled receptors: structure- and function-based drug
747 discovery. *Signal Transduct Target Ther* **6**, 7 (2021).
748 4. Wootten, D., Christopoulos, A., Marti-Solano, M., Babu, M. M. & Sexton, P. M.
749 Mechanisms of signaling and biased agonism in G protein-coupled receptors.
750 *Nat Rev Mol Cell Biol* **19**, 638–653 (2018).
751 5. Shenoy, S. K. & Lefkowitz, R. J. β-arrestin-mediated receptor trafficking and
752 signal transduction. *Trends Pharmacol Sci* **32**, 521–533 (2011).
753 6. Pin, J.-P. *et al.* International Union of Basic and Clinical Pharmacology. LXVII.
754 Recommendations for the Recognition and Nomenclature of G Protein-Coupled
755 Receptor Heteromultimers. *Pharmacol Rev* **59**, 5 LP – 13 (2007).
756 7. Ferré, S. *et al.* G protein-coupled receptor-effector macromolecular membrane
757 assemblies (GEMMAs). *Pharmacol Ther* **231**, 107977 (2022).
758 8. Angers, S. *et al.* Detection of β2-adrenergic receptor dimerization in living cells
759 using bioluminescence resonance energy transfer (BRET). *Proceedings of the*
760 *National Academy of Sciences* **97**, 3684–3689 (2000).
761 9. Whorton, M. R. *et al.* A monomeric G protein-coupled receptor isolated in a high-
762 density lipoprotein particle efficiently activates its G protein. *Proceedings of the*
763 *National Academy of Sciences* **104**, 7682–7687 (2007).
764 10. Asher, W. B. *et al.* Single-molecule FRET imaging of GPCR dimers in living cells.
765 *Nat Methods* **18**, 397–405 (2021).
766 11. Ferré, S. *et al.* G protein-coupled receptor oligomerization revisited: Functional
767 and pharmacological perspectives. *Pharmacological Reviews* **66**, 413–434
768 (2014).
769 12. Ferré, S. *et al.* Building a new conceptual framework for receptor heteromers.
770 *Nature Chemical Biology,* **5***,* 131–134*.* (2009).
771 13. Kasai, R. S. & Kusumi, A. Single-molecule imaging revealed dynamic GPCR
772 dimerization. *Curr Opin Cell Biol* **27**, 78–86 (2014).

773 14. Tabor, A. *et al.* Visualization and ligand-induced modulation of dopamine
774 receptor dimerization at the single molecule level. *Sci Rep* **6***,* 33233 (2016).
775 15. Calebiro, D. *et al.* Single-molecule analysis of fluorescently labeled G-protein–
776 coupled receptors reveals complexes with distinct dynamics and organization.
777 *Proceedings of the National Academy of Sciences* **110**, 743–748 (2013).
778 16. Hern, J. A. *et al.* Formation and dissociation of M1 muscarinic receptor dimers
779 seen by total internal reflection fluorescence imaging of single molecules.
780 *Proceedings of the National Academy of Sciences* **107**, 2693–2698 (2010).
781 17. Milligan, G. The role of dimerisation in the cellular trafficking of G-protein-coupled
782 receptors. *Curr Opin Pharmacol* **10**, 23–29 (2010).
783 18. Ferre, S., Von Euler, G., Johansson, B., Fredholm, B. B. & Fuxe, K. Stimulation
784 of high-affinity adenosine A2 receptors decreases the affinity of dopamine D2
785 receptors in rat striatal membranes. *Proc Natl Acad Sci U S A* **88,** 7238–7241
786 (1991).
787 19. Ge, B. *et al.* Single-molecule imaging reveals dimerization/oligomerization of
788 CXCR4 on plasma membrane closely related to its function. *Sci Rep* **7**, 16873
789 (2017).
790 20. Rodríguez-Frade, J. M., Mellado, M. & Martínez-A, C. Chemokine receptor
791 dimerization: two are better than one. *Trends Immunol* **22**, 612–617 (2001).
792 21. Liu, J. *et al.* Biased signaling due to oligomerization of the G protein-coupled
793 platelet-activating factor receptor. *Nat Commun* **13**, 6365 (2022).
794 22. Sun, Y. *et al.* Single-molecule imaging reveals the stoichiometry change of β2-
795 adrenergic receptors by a pharmacological biased ligand. *Chem. Commun.* **52**,
796 7086–7089 (2016).
797 23. Gusach, A., García-Nafría, J. & Tate, C. G. New insights into GPCR coupling
798 and dimerisation from cryo-EM structures. *Curr Opin Struct Biol* **80**, 102574
799 (2023).
800 24. Neve, K. A., Seamans, J. K. & Trantham-Davidson, H. Dopamine Receptor
801 Signaling. *J Recept Signal Transduct Res* **24***,* 165–205 (2004).
802 25. Missale, C., NASH, S. R., ROBINSON, S. W., JABER, M. & CARON, M. G.
803 Dopamine Receptors: From Structure to Function. *Physiol Rev* **78**, 189–225
804 (1998).

805 26. Beaulieu, J.-M. & Gainetdinov, R. R. The Physiology, Signaling, and
806 Pharmacology of Dopamine Receptors. *Pharmacol Rev* **63**, 182 LP – 217
807 (2011).
808 27. Albizu, L. *et al.* Time-resolved FRET between GPCR ligands reveals oligomers
809 in native tissues. *Nat Chem Biol* **6**, 587–594 (2010).
810 28. Guo, W. *et al.* Dopamine D2 receptors form higher order oligomers at
811 physiological expression levels. *EMBO Journal* **27**, 2293-304 (2008).
812 29. Kasai, R. S., Ito, S. V, Awane, R. M., Fujiwara, T. K. & Kusumi, A. The Class-A
813 GPCR Dopamine D2 Receptor Forms Transient Dimers Stabilized by Agonists:
814 Detection by Single-Molecule Tracking. *Cell Biochem Biophys* **76**, 29–37 (2018).
815 30. Wang, M. *et al.* Schizophrenia, amphetamine-induced sensitized state and acute
816 amphetamine exposure all show a common alteration: increased dopamine D2
817 receptor dimerization. *Mol Brain* **3**, 25 (2010).
818 31. Masri, B. *et al.* Antagonism of dopamine D2 receptor/β-arrestin 2 interaction is a
819 common property of clinically effective antipsychotics. *Proc Natl Acad Sci U S A*
820 **105**, 13656–13661 (2008).
821 32. Wang, S. *et al.* Structure of the D2 dopamine receptor bound to the atypical
822 antipsychotic drug risperidone. *Nature* **555**, 269 (2018).
823 33. Fan, L. *et al.* Haloperidol bound D2 dopamine receptor structure inspired the
824 discovery of subtype selective ligands. *Nat Commun* **11**, 1074 (2020).
825 34. Yin, J. *et al.* Structure of a D2 dopamine receptor-G-protein complex in a lipid
826 membrane. *Nature* **584**, 125 (2020).
827 35. Buenaventura, T. *et al.* Agonist-induced membrane nanodomain clustering
828 drives GLP-1 receptor responses in pancreatic beta cells. *PLoS Biol* **17**,
829 e3000097 (2019).
830 36. Casarini, L. *et al.* Membrane Estrogen Receptor (GPER) and Follicle-Stimulating
831 Hormone Receptor (FSHR) Heteromeric Complexes Promote Human Ovarian
832 Follicle Survival. *iScience* **23**, (2020).
833 37. Walker, A. R. *et al.* Functional rewiring of G protein-coupled receptor signaling
834 in human labor. *Cell Rep* **40**, (2022).
835 38. Jonas, K. C., Fanelli, F., Huhtaniemi, I. T. & Hanyaloglu, A. C. Single Molecule
836 Analysis of Functionally Asymmetric G Protein-coupled Receptor (GPCR)
837 Oligomers Reveals Diverse Spatial and Structural Assemblies. *Journal of*
838 *Biological Chemistry* **290**, 3875–3892 (2015).

839 39. Jonas, K. C. *et al.* Temporal reprogramming of calcium signaling via crosstalk of
840 gonadotrophin receptors that associate as functionally asymmetric heteromers.
841 *Sci Rep* **8**, 2239 (2018).
842 40. Beaulieu, J. M. *et al.* An Akt/β-arrestin 2/PP2A signaling complex mediates
843 dopaminergic neurotransmission and behavior. *Cell* **122**, 261 (2005).
844 41. Skinbjerg, M. *et al.* Arrestin3 mediates D2 dopamine receptor internalization.
845 *Synapse* **63**, 621–624 (2009).
846 42. Allen, J. A. *et al.* Discovery of β-Arrestin–Biased Dopamine D2 Ligands for
847 Probing Signal Transduction Pathways Essential for Antipsychotic Efficacy.
848 *Proceedings of the National Academy of Sciences* **108**, 18488–18493 (2011).
849 43. Urs, N. M. *et al.* Distinct cortical and striatal actions of a β-arrestin–biased
850 dopamine D2 receptor ligand reveal unique antipsychotic-like properties.
851 *Proceedings of the National Academy of Sciences* **113**, E8178–E8186 (2016).
852 44. Shukla, A. K., Xiao, K. & Lefkowitz, R. J. Emerging paradigms of β-arrestin-
853 dependent seven transmembrane receptor signaling. *Trends Biochem Sci* **36**,
854 457–469 (2011).
855 45. DeWire, S. M., Ahn, S., Lefkowitz, R. J. & Shenoy, S. K. β-Arrestins and Cell
856 Signaling. *Annu Rev Physiol* **69**, 483–510 (2007).
857 46. Shenoy, S. K. & Lefkowitz, R. J. β-arrestin-mediated receptor trafficking and
858 signal transduction. *Trends Pharmacol Sci* **32**, 521–533 (2011).
859 47. Han, Y., Moreira, I. S., Urizar, E., Weinstein, H. & Javitch, J. A. Allosteric
860 communication between protomers of dopamine class A GPCR dimers
861 modulates activation. *Nat Chem Biol* **5**, 688–695 (2009).
862 48. Maharana, J. *et al.* Structural snapshots uncover a key phosphorylation motif in
863 GPCRs driving β -arrestin activation. *Mol Cell* **83**, 2091-2107.e7 (2023).
864 49. Huang, J., Chen, S., Zhang, J. J. & Huang, X. Y. Crystal structure of oligomeric
865 β 1-adrenergic G protein-coupled receptors in ligand-free basal state. *Nat Struct*
866 *Mol Biol* **20**, 419–425 (2013).
867 50. Salom, D. *et al.* Crystal structure of a photoactivated deprotonated intermediate
868 of rhodopsin. *Proceedings of the National Academy of Sciences* **103**, 16123 LP
869 – 16128 (2006).
870 51. Manglik, A. *et al.* Crystal structure of the μ-opioid receptor bound to a morphinan
871 antagonist. *Nature* **485**, 321–326 (2012).

872 52. Wu, H. *et al.* Structure of the human κ-opioid receptor in complex with JDTic.
873 *Nature* **485**, 327–332 (2012)
874 53. Yue, Y. *et al.* Structural insight into apelin receptor-G protein stoichiometry. *Nat*
875 *Struct Mol Biol* **29**, 688–697 (2022).
876 54. Guo, W., Shi, L. & Javitch, J. A. The fourth transmembrane segment forms the
877 interface of the dopamine D2 receptor homodimer. *Journal of Biological*
878 *Chemistry* **278**, 4385–4388 (2003).
879 55. Bueschbell, B. *et al.* The World of GPCR dimers: Mapping dopamine receptor
880 D_2 homodimers in different activation states and configuration arrangements.
881 *Comput Struct Biotechnol J* **21**, 4336–4353 (2023).
882 56. Johnston, J. M. *et al.* Making Structural Sense of Dimerization Interfaces of Delta
883 Opioid Receptor Homodimers. *Biochemistry* **50**, 1682–1690 (2011).
884 57. Pulido, D. *et al.* Design of a True Bivalent Ligand with Picomolar Binding Affinity
885 for a G Protein-Coupled Receptor Homodimer. *J Med Chem* **61**, 9335–9346
886 (2018).
887 58. Lane, J. R., May, L. T., Parton, R. G., Sexton, P. M. & Christopoulos, A. A kinetic
888 view of GPCR allostery and biased agonism. *Nat Chem Biol* **13**, 929–937 (2017).
889 59. Seyedabadi, M., Ghahremani, M. H. & Albert, P. R. Biased signaling of G protein
890 coupled receptors (GPCRs): Molecular determinants of GPCR/transducer
891 selectivity and therapeutic potential. *Pharmacol Ther* **200**, 148–178 (2019).
892 60. Grimes, J. et al. Plasma membrane preassociation drives β-arrestin coupling to
893 receptors and activation. *Cell* **186**, 2238-2255.e20 (2023).
894 61. Damian, M. *et al.* Allosteric modulation of ghrelin receptor signaling by lipids. *Nat*
895 *Commun* **12**, 3938 (2021).
896 62. Dawaliby, R. *et al.* Allosteric regulation of G protein–coupled receptor activity by
897 phospholipids. *Nat Chem Biol* **12**, 35–39 (2016).
898 63. Hanson, M. A. *et al.* A Specific Cholesterol Binding Site Is Established by the 2.8
899 Structure of the Human & β 2-Adrenergic Receptor. *Structure* **16**, 897–905
900 (2008).
901 64. Kockelkoren, G. *et al.* Molecular mechanism of GPCR spatial organization at the
902 plasma membrane. *Nat Chem Biol* **20**, 142–150 (2023).
903 65. Gahbauer, S. & Böckmann, R. A. Membrane-Mediated Oligomerization of G
904 Protein Coupled Receptors and Its Implications for GPCR Function. *Frontiers in*
905 *Physiology* **7**, 494 (2016).

906 66. Quan, W., Kim, J.-H., Albert, P. R., Choi, H. & Kim, K.-M. Roles of G protein and
907 β-arrestin in dopamine D2 receptor-mediated ERK activation. *Biochem Biophys*
908 *Res Commun* **377**, 705–709 (2008).
909 67. Kim, S. J., Kim, M. Y., Lee, E. J., Ahn, Y. S. & Baik, J. H. Distinct regulation of
910 internalization and mitogen-activated protein kinase activation by two isoforms
911 of the dopamine D2 receptor. *Molecular Endocrinology* **3**, 640–652 (2004).
912 68. Maharana, J. *et al.* Molecular insights into atypical modes of β-arrestin
913 interaction with seven transmembrane receptors. *Science* **383**, 101–108 (2024).
914 69. Mores, K. L., Cassell, R. J. & van Rijn, R. M. Arrestin recruitment and signaling
915 by G protein-coupled receptor heteromers. *Neuropharmacology* **152**, 15–21
916 (2019).
917 70. Borroto-Escuela, D. O. *et al.* On the existence of a possible A2A-D2-β- arrestin2
918 complex: A2A agonist modulation of D2 agonist-induced β-arrestin2 recruitment.
919 *J Mol Biol* **406**, 687-99 (2011).
920 71. White, J. F. *et al.* Dimerization of the class A G protein-coupled neurotensin
921 receptor NTS1 alters G protein interaction. *Proceedings of the National Academy*
922 *of Sciences* **104**, 12199–12204 (2007).
923 72. Arcemisbéhère, L. *et al.* Leukotriene BLT2 Receptor Monomers Activate the G_{i2}
924 GTP-binding Protein More Efficiently than Dimers . *Journal of Biological*
925 *Chemistry* **285**, 6337–6347 (2010).
926 73. Maurice, P., Kamal, M. & Jockers, R. Asymmetry of GPCR oligomers supports
927 their functional relevance. *Trends Pharmacol Sci* **32**, 514–520 (2011).
928 74. Huang, L., Wu, D., Zhang, L. & Feng, L. Modulation of A2a receptor antagonist
929 on D2 receptor internalization and ERK phosphorylation. *Acta Pharmacol Sin* **34**,
930 1292–1300 (2013).
931 75. Bonaventura, J. *et al.* Allosteric interactions between agonists and antagonists
932 within the adenosine A2a; receptor-dopamine D2 receptor heterotetramer.
933 *Proceedings of the National Academy of Sciences* **112**, E3609 LP-E3618 (2015).
934 76. Fuxe, K. *et al.* Adenosine-dopamine interactions in the pathophysiology and
935 treatment of cns disorders. *CNS Neuroscience and Therapeutics* Preprint at
936 https://doi.org/10.1111/j.1755-5949.2009.00126.x (2010).
937 77. Fernández-Dueñas, V. *et al.* Revealing Adenosine A(2A)-Dopamine D(2)
938 Receptor Heteromers in Parkinson's Disease Post-Mortem Brain through a New
939 AlphaScreen-Based Assay. *Int J Mol Sci* **20**, 3600 (2019).

78. Fanelli, F., Hanyaloglu, A. C. & Jonas, K. Chapter Five - Integrated structural modeling and super-resolution imaging resolve GPCR oligomers. in *Oligomerization in Health and Disease: From Enzymes to G Protein-Coupled Receptors* (eds. Giraldo, J. & Ciruela, F. B. T.-P. in M. B. and T. S.) vol. 169 151–179 (Academic Press, 2020).
79. Casciari, D., Seeber, M. & Fanelli, F. Quaternary structure predictions of transmembrane proteins starting from the monomer: a docking-based approach. *BMC Bioinformatics* **7**, 340 (2006).
80. Fanelli, F., Seeber, M., Felline, A., Casciari, D. & Raimondi, F. Chapter Five - Quaternary Structure Predictions and Structural Communication Features of GPCR Dimers. in *Oligomerization in Health and Disease* (eds. Giraldo, J. & Ciruela, F. B. T.-P. in M. B. and T. S.) vol. 117 105–142 (Academic Press, 2013).
81. Chen, R., Li, L. & Weng, Z. ZDOCK: An initial-stage protein-docking algorithm. *Proteins: Structure, Function, and Bioinformatics* **52**, 80–87 (2003).
82. Hwang, H., Pierce, B., Mintseris, J., Janin, J. & Weng, Z. Protein–protein docking benchmark version 3.0. *Proteins: Structure, Function, and Bioinformatics* **73**, 705–709 (2008).
83. Sali, A. & Blundell, T. L. Comparative protein modelling by satisfaction of spatial restraints. *J Mol Biol* **234**, 779–815 (1993).
84. Hoare, S. R. J. *et al.* Quantifying the Kinetics of Signaling and Arrestin Recruitment by Nervous System G-Protein Coupled Receptors. *Front Cell Neurosci* **15**, (2022).
85. Henriques, R. *et al.* QuickPALM: 3D real-time photoactivation nanoscopy image processing in ImageJ. *Nat Methods* **7**, 339–340 (2010).

968

969 ## Acknowledgements

970 We would like to acknowledge Drs Stephen Rothery and David Gaboriau at the Facility
971 for Imaging of Light Microscopy at Imperial College London for their technical support
972 for microscopy experiments. Dr. Asuka Inoue (Univ. Tohoku, Japan) for supplying the
973 β-arrestin1/2 KO cell line. Frederic Jean-Alphonse (CNRS, Nouzilly) for β-arrestin-YFP
974 plasmids, Jonathan Javitch (Univ. Columbia, USA) for WT D_2R plasmids. We would
975 like to acknowledge the use of Biorender.com for the production of schematic figures.
976 This project was funded by Biotechnology and Biological Sciences Research Council
977 (Grant BB/M011178/1).

978

979 ## Author contributions

980 B.B and A.C.H conceived the study and with K.L.S designed the experiments. K.L.S
981 performed the majority of wet laboratory experiments, analysis and figure preparation
982 with contributions from Y.L for certain βarr BRET recruitment assays and molecular
983 biology; A.J.M for certain cAMP assays; W.Y for some confocal microscopy imaging.
984 F.F performed all molecular modelling and analysis. K.L.S wrote the majority of the
985 manuscript with A.C.H and B.B. F.F wrote the sections of the manuscript relating to
986 molecular modelling, with inputs and review by K.L.S, B.B and A.C.H. All authors
987 contributed to and approved the final manuscript.

988

Table 1. Quinpirole potency in cAMP and βarr2 BRET recruitment assays shown as $-\log EC_{50}$. Data shown with 95% confidence interval (CI). Two-tailed, unpaired Student's t-test used to determine statistical significance between WT and mutant $-\log EC_{50}$ values (p*=0.0147 (V96C) or 0.0433 (V96S)).

Receptor	cAMP -log EC_{50}	βarr2 recruitment -log EC_{50}
D_2R WT	-9.418 (CI -9.761 to -9.073)	-5.362 (CI -5.527 to-5.196)
D_2R V96C	-9.036 (CI -9.535 to -8.546)	-5.695 (CI -5.814 to -5.576)*
D_2R V96S	-9.275 (CI -10.280 to -8.358)	-5.804 (CI -6.044 to -5.565)*
D_2R V96S/V97C	-9.490 (-10.270 to -8.687)	-5.622 (-5.788 to -5.457)
D_2R V97C	-9.225 (CI -10.020 to -8.357)	5.626 (CI -5.167 to -6.0850)
D_2R Y93C	-9.547 (-10.180 to -8.920)	5.435 (CI 5.242 to 5.628)

Table 2. Quinpirole- induced βarr2 BRET recruitment kinetics. Rate (k), initial rate, halftime and plateau were calculated following curve fitting from the waveform produced from ligand-induced BRET recruitment assays (Supplementary Fig.6). Data is presented with 3 different D_2R WT data sets, to allow comparisons with mutant D_2R experiments that were carried out at the same time under the same experimental conditions. N=4-6, data shown as +/- SEM. Two-tailed, unpaired Student's t-test used to determine statistical significance between WT and mutant $-\log IC_{50}$ values (p**= 0.0014 or 0.0068).

	k (second-1)	Initial Rate (BRET ratio units per second)	Half time (seconds)	Plateau
WT	1.076×10^{-2} ($\pm 1.283 \times 10^{-3}$)	5.27×10^{-4} ($\pm 1.644 \times 10^{-4}$)	68.38 (±8.537)	0.04908 ($\pm 1.166 \times 10^{-2}$)
V96C	1.999×10^{-2} ($\pm 1.446 \times 10^{-3}$)**	1.002×10^{-3} ($\pm 1.842 \times 10^{-4}$)	35.55 (±3.058)**	0.05012 ($\pm 8.027 \times 10^{-3}$)
WT	4.754×10^{-3} ($\pm 3.549 \times 10^{-3}$)	1.579×10^{-4} ($\pm 1.049 \times 10^{-4}$)	30.28(±4.99)	0.03682 ($\pm 7.335 \times 10^{-3}$)
Y93C	3.33×10^{-3} ($\pm 1.943 \times 10^{-3}$)	1.135×10^{-4} ($\pm 5.866 \times 10^{-5}$)	34.57(±14.05)	0.03119 ($\pm 7.849 \times 10^{-3}$)
V97C	4.434×10^{-3} ($\pm 3.577 \times 10^{-3}$)	1.807×10^{-4} ($\pm 1.499 \times 10^{-4}$)	32.66 (±4.764)	0.0297 ($\pm 6.017 \times 10^{-3}$)
WT	3.065×10^{-2} ($\pm 1.072 \times 10^{-2}$)	8.603×10^{-4} ($\pm 5.241 \times 10^{-4}$)	41.08(± 7.252)	0.02122 ($\pm 5.301 \times 10^{-3}$)
V96S	2.702×10^{-2} ($\pm 8.711 \times 10^{-3}$)	7.002×10^{-4} ($\pm 3.117 \times 10^{-4}$)	39.36 (± 8.69)	0.02394 ($\pm 3.826 \times 10^{-3}$)

989

990

991

992